AD734701

Institute of Oceanography
Old Dominion University
Norfolk, Virginia

12

Technical Report No. 2

Migration of Tidal Sand Waves in Chesapeake Bay Entrance

by

John C. Ludwick

Technical Report obtained under
Contract Number N00014-70-C-0083,
Task Number NR 388-098 of the
Geography Program Branch,
Office of Naval Research.

November 15, 1971

74

UNCLASSIFIED
Security Classification

DOCUMENT CONTROL DATA - R & D

(Security classification of title, body of abstract and indexing annotation must be entered when the overall report is classified)

1. ORIGINATING ACTIVITY (Corporate author)
Institute of Oceanography
Old Dominion University
Norfolk, Virginia 23508

2a. REPORT SECURITY CLASSIFICATION
Unclassified

2b. GROUP

3. REPORT TITLE
Migration of Tidal Sand Waves in Chesapeake Bay Entrance

4. DESCRIPTIVE NOTES (Type of report and inclusive dates)
Technical Report

5. AUTHOR(S) (First name, middle initial, last name)
John C. Ludwick

6. REPORT DATE
November 15, 1971

7a. TOTAL NO OF PAGES
89

7b. NO OF REFS
78

8a. CONTRACT OR GRANT NO
N00014-70-C-0083

b. PROJECT NO.
NR 388-098

c.

d.

9a. ORIGINATOR'S REPORT NUMBER(S)
Technical Report No. 2

9b. OTHER REPORT NO(S) (Any other numbers that may be assigned this report)

10. DISTRIBUTION STATEMENT
This document has been approved for public release and sale; its distribution is unlimited.

11. SUPPLEMENTARY NOTES

12. SPONSORING MILITARY ACTIVITY
Geography Branch
Office of Naval Research
Washington, D. C.

13. ABSTRACT
Subtidal sand waves occur atop shoals and on shoal margins in the northern part of the tidal entrance to Chesapeake Bay, Virginia. Wavelength ranges from 200-800 ft; height ranges from 5-11 ft. All major slopes are 2-3°, far less than the angle of repose of the constituent sediment. In flood-dominated tidal channels, sand waves are asymmetrical and face landwards; in ebb-dominated tidal channels and atop most banks, sand waves face seawards. Where near-bottom flood and ebb tidal currents are equal in time-velocity impulse, sand waves of symmetrical trochoidal profile are developed.

Data from 21 successive echo-sounding profiles taken over a 17-month period show that the seaward-facing asymmetrical sand waves are migrating seaward. Rates of migration of these waves range from 115 to 492 ft/year. Symmetrical sand waves did not show significant migration. Sand wave height changes seasonally, trochoidal waves experiencing a two-fold height change. Small heights occur from October to late April when suface water waves are frequently higher than 5 ft; large sand wave heights occur from May to September particularly during the latter month when surface water waves are usually lower than 5 ft in height.

Prominent shoals in the entrance area characteristically have ebb-dominated near-bottom tidal currents on one side and flood-dominated near-bottom tidal currents on the other side. This pattern is suggestive of a sand circulation conjoint with the shoal.

DD FORM 1 NOV 65 1473 (PAGE 1)

S/N 0101-807-6801

UNCLASSIFIED
Security Classification

14 KEY WORDS	LINK A		LINK B		LINK C	
	ROLE	WT	ROLE	WT	ROLE	WT
Sand waves						
Tidal currents						
Estuary entrance						
Shoal development						
Sediment						

Institute of Oceanography
Old Dominion University
Norfolk, Virginia 23508

Technical Report No. 2

Migration of Tidal Sand Waves in
Chesapeake Bay Entrance

By

John C. Ludwick

Technical Report obtained under
Contract Number N000-14-70-C-0083,
Task Number NR 388-098, of the
Geography Programs Branch,
Office of Naval Research.

November 15, 1971

ABSTRACT

Subtidal sand waves occur atop shoals and on shoal margins in the northern part of the tidal entrance to Chesapeake Bay, Virginia. Wave length ranges from 200-800 ft; height ranges from 5-11 ft. All major slopes are 2-3^{o}, far less than the angle of repose of the constituent sediment. In flood-dominated tidal channels, sand waves are asymmetrical and face landwards; in ebb-dominated tidal channels and atop most banks, sand waves face seawards. Where near-bottom flood and ebb tidal currents are equal in time-velocity impulse, sand waves of symmetrical-trochoidal profile are developed.

Data from 21 successive echo-sounding profiles taken over a 17-month period show that the seaward-facing asymmetrical sand waves are migrating seaward. Rates of migration of these waves range from 115 to 492 ft/year. Symmetrical sand waves did not show significant migration. Sand wave height changes seasonally, trochoidal waves experiencing a two-fold height change. Small heights occur from October to late April when surface water waves are frequently higher than 5 ft; large sand wave heights occur from May to September, particularly during the latter month when surface water waves are usually lower than 5 ft in height.

Prominent shoals in the entrance area characteristically have ebb-dominated near-bottom tidal currents on one side and flood-dominated near-bottom tidal currents on the other side. This pattern is suggestive of a sand circulation conjoint with the shoal. Geomorphic evidence is consistent with the existence of such sand circulation cells. The circulation mechanism would explain how the shoals maintain their positions in the face of strong tidal currents and heavy wave action.

ACKNOWLEDGMENT

Several faculty members and graduate students of the Institute of Oceanograpy, Old Dominion University, participated along with the author in some of the work reported. They include Drs. D. J. P. Swift, R. E. Johnson, and graduate students, W. C. Smith, J. R. Wells, J. R. Melchor. Captains of R/V ALBATROSS and R/V LINWOOD HOLTON were helpful in accomplishing the objectives.

CONTENTS

FIGURES

Figure

TABLES

BLANK PAGE

Introduction

At present, the migration rate of subtidal sand waves is most readily obtained from comparisons made between at least two successive bathymetric surveys in which corresponding sand wave crests can be confidently identified. More than two runs are required to detect and to reach conclusions about the cause of an increase or decrease in sand wave migration rate. In the present study a series of 21 successive profiles taken over a period of 17 months are examined for evidence of the effects of tidal phase, run-off, and wave action. The ubiquity of sand waves in tidal inlets and entrances, port approaches, navigation channels, as well as the probable role of sand waves in shoal evolution, sediment movement, and burial of minefields would appear to warrant an analysis of travel rates.

Even in the very earliest studies of undulose bed forms, migration rate was seen to vary with fluid flow velocity. Before 1871 an empirical equation had been developed in which sand bank travel rate was related to the square of the surface flow velocity (Leliavsky, 1955, p. 12). This expression (Fig. 1) was deduced by the French engineer, Sainjon, from observations in the Loire River. Chang (1939) and Salsman, et al. (1966) have presented other migration data from flume and field that are fitted by fifth power functions of flow velocity. Allen (1963) reduced the Loire River migration data of Ballade (1953) to a power function in which the fluid flow velocity bears the exponent, 2.41. Although flow velocity is probably the single factor that produces the largest effect on sand wave migration rate, other factors are obviously of considerable significance.

Sand wave migration is perhaps more purposively associated with the movement of bed sediment than with fluid flow velocity. Unfortunately, here it is seen that all the unsolved problems of initiation of sediment motion, turbulent transport, and non-Newtonian behavior of sediment-ladened suspensions are obstacles to a full physical understanding of sand wave travel rate. It can be deduced readily that among the relevant factors are: 1) particle properties including density, size, shape, and cohesion; 2) fluid properties, including density, viscosity, and therefore temperature; 3) boundary properties, including roughness, sand wave height, wave length, and bed slope; and finally, 4) water depth or depth below an internal fluid flow boundary. The shear stress exerted by the moving fluid on the bed is a key factor in sediment transport and in sand wave migration.

In most studies of sand wave migration rate, detailed consideration of cause of migration is usually preceded by a determination of flow regime (Deacon, 1894; Gilbert, 1914; Simons et al., 1961, 1965), since in the upper regime, the direction of motion of the bed forms may even be opposite to the direction of the fluid flow. Kennedy (1963, 1969) gives the following expression for the minimum Froude number at which antidunes form: $F^2 = (1/kd)\tanh kd$ The symbols are defined below. This lower limit is seen to depend on kd, water depth relative to wave length.

The migration rate equation that follows was also developed by Kennedy (1969) and illustrates for the two-dimensional case, the plurality of factors relevant to travel rate of fully-developed bed forms:

$$U_b = (\bar{T}_b/\beta) nk \, [U/(U - U_c)] \, [(1 - F^2 \, kd \tanh kd)/(\tanh kd - F^2 \, kd)],$$

where U_b is bed form migration velocity; $\bar{T}_b$ is the average volume rate, per unit width of channel, of downstream sediment transport due only to the migration of bed sediment; β (taken as unity by Kennedy in a sample computation) is the ratio of bed load to total sediment transport; n (taken as 2.64 in a sample computation for sediment 0.93 mm in mean size) is a dimensionless exponent in an assumed sediment transport law; k is the wave number, $2\pi/L$, where L is wave length; U is unidirectional mean fluid flow velocity; U_c (taken as 1.30 ft/sec in a sample computation for sediment 0.93 mm in mean size) is the critical velocity for initiation of motion; and F is the Froude number, $U/\sqrt{gd}$, where g is gravitational acceleration, and d is water depth.

Under strong, but subcritical, unidirectional flow, profiles of actively moving undulose bed forms are asymmetrical, and often exhibit steep downstream faces which slope at the underwater angle of repose of the constituent sediment. This angle ranges from 24 to 34 degrees. Under reversing flow, as in tidal channels, if ebb and flood currents are of equal strength and duration, symmetrical bed form profiles of trochoidal shape are developed. Forel (1883) regarded profiles of this type as composites of two asymmetrical opposed forms. Profiles of intermediate symmetry, produced when ebb and flood currents are not equal in strength and duration, are aptly termed asymmetrical-trochoidal (Van Veen, 1935).

Migration of strongly asymmetrical forms with slip faces occurs by bed erosion on the upstream slope of the wave and by deposition on the downstream face which builds forward by intermittent or continuous avalanching of sediment (Allen, 1962, 1965; Jopling, 1965; Harms, 1969). Small symmetrical forms on a level bottom may oscillate under reversing flow, but do not undergo net translation. Bed waves that are asymmetrical-trochoidal in profile migrate in the direction of the net, or residual, current and are steeper downstream of the dominating current.

Increasingly evidence is coming to light that miaximum slopes of many large sand waves are considerably less than the angle of repose of the constituent sediment (Bucher, 1919; Lane and Eden, 1940; Carey and Keller, 1957; Cartwright, 1959; Allen, 1963; Visher, 1965; Imbrie and Buchanan, 1965). It seems likely that there is no boundary layer separation of the flow at the subdued crests of such features, no persistent lee eddy, and no lee counter current. Under a competent unidirectional flow, sediment at the bed would be transported unidirectionally along the entire form profile. The origin and maintenance of low-slope sand waves are unclear.

Large sand waves advance more slowly than small sand waves of identical profile if the bed sediment transport rate per unit width of channel is the same for both features (Cornish, 1901; Cloet, 1954a, b; Simons and Richardson, 1960; Allen, 1965; Ashida and Tanaka, 1967; Crickmore, 1970). Smith (1968) and Nordin (1968) concluded that sand waves of short wave length migrate faster than those of longer wave length. The preferred explanation is that large sand waves have a large sediment storage volume and thus require more sediment to move a unit distance. A consequence of the rapid movement of small bed forms is that they overtake larger features in the same wave train, merge with them, increase the size of the larger forms, and increase the incidence of long wave lengths by decreasing the incidence of short wave lengths. Some investigators have argued that sand wave height should therefore increase among the forms in a wave train with distance in the direction of migration. It is a corollary of this idea that larger sand waves are older waves.

Sand wave migration rates vary seasonally in some estuaries and tidal rivers. In the Loire River, Ballade (1953) found that during the season of low run-off, sand waves at Ile de Bois, 32 km from the mouth of the river, experienced only back and forth excursions of 3 to 8 meters and only the tops of the bed features were affected. During the season of high run-off, the ebb current was aided, sand wave asymmetry developed, and the entire train migrated downstream at a rate of 2.5 m/day under peak discharge.

The migration of sand waves and the evolution of some sediment shoals are apparently related. Using the then newly-developed recording echo-sounder, Van Veen (1935, 1936) showed that the great current-parallel sand ridges of the southern North Sea were surmounted by sand waves. Earlier, Cornish (1901) had noted in his study of intertidal shoals and sand waves of English estuaries, that there was a clear correspondence between the facing direction of asymmetrical sand waves and the asymmetry of the shoals that they surmounted.

Following the firm establishment by Cornish (1901) of the finding that ebb-dominant and flood-dominant currents tend to be at least partly confined to different, mutually evasive channels among tidal shoals, and the related finding by Van Veen that parabolic-shaped shoals were a fundamental form conjoint with this distribution of currents, Van Straaten (1950, 1953) showed that sand waves found in the tidal channels between limbs of parabolas faced the closed or dead-ends of the channels. He also showed that in the tidal channels on either side of a linear shoal, sand waves faced with the dominant current and in opposite directions.

It would now appear likely that many sand shoals subject to mutually evasive tidal flows are coexistent with sand circulation cells the presence of which is revealed by the mapped pattern of sand wave facing directions (Houbolt, 1968; Smith, 1968, 1969; James and Stanley, 1968; Klein, 1970). Other sand banks subject to tidal currents appear to owe their existence to the convergent motion of sand waves from opposite sides of the banks (Jordan, 1962; Dingle, 1965; Jones, Kain, and Stride, 1965). Alternate exposure and shielding of the two sides of the bank to ebb and flood currents account for the observed disposition of the asymmetrical sand waves.

Certain fields of large asymmetrical sand waves in the North Sea off the Netherlands did not experience migration within detectable limits of 60 m over a survey period of 2.5 years (Langeraar, 1966; Anonymous, 1967); however, this is possibly an indication of a slow rate of migration. Other workers in the seas surrounding the British Isles have mapped in considerable detail probable regional sand distribution pathways from the facing directions of sand waves (Stride and Cartwright, 1958; Stride, 1963; Belderson and Stride, 1966; Harvey, 1966; Kenyon and Stride, 1968; Terwindt, 1971). Dominant tidal currents and sand wave facing direction are strongly correlated.

Field Area and Methods

The present study was performed in the entrance area of Chesapeake Bay, the largest estuary on the Atlantic Coast of the United States (Fig. 2).

Physiographically the water body is a coastal plain estuary formed by drowning of a Pleistocene-incised river valley. The estuary is approximately 314 km long and 24 km in average width in the lower reaches. Water depth in the lower part of the bay is 9.1 m and in the entrance area averages 11.1 m. Fresh water river inflow averages 1500 m^3/sec. Salinity in the entrance area ranges from 18 ‰ to 33 ‰ seasonally.

The distance between the capes at the mouth of the estuary is 18 km. Two principal shipping channels pass through this entrance; Thimble Shoal Channel, the approach to which is 25.3 m deep; and Chesapeake Channel which is 15.8 m deep. In the northern half of the entrance area there is a complex array of subtidal sand banks and intervening tidal channels. Water depth to the top of these banks ranges from 1 to 5 m relative to MLW. Water depth in the deepest parts of the channels ranges from 10 to 20 m. By following a zigzag path it is possible to move from the north side of the entrance to within 4 km of the south headland without entering water deeper than 7.3 m. This is possible because of the serpentine shape of the shoals and the position of some shoals in a blocking position athwart main channels.

Chesapeake Bay is unique in that it is sufficiently long to accommodate one semidiurnal tidal wave at all times. Owing to frictional losses there is very nearly no reflected wave felt in the entrance area and hence the tide there is of the progressive type: maximum tidal currents are nearly synchronous with high water and low water. Mean tidal range at the north side of the entrance is 0.89 m. At the south side it is 0.86 m. At spring tide the corresponding ranges are 1.10 m and 1.04 m. Duration of fall exceeds duration of rise on the northern side of the entrance in contrast to the south side.

Surface tidal currents in the entrance area of the bay, range from 50 to 100 cm/sec at ebb and flood maxima on most days. The greatest annual forecasted surface current at any place in the entrance is 175 cm/sec. This is in the channel west of Fisherman Island (Fig. 3) and occurs on a flood current. Annual maximum ebb current for the entrance occurs in the same channel but is only 140 cm/sec.

There are pronounced differences in ebb current speed and flood current speed at different places in the entrance. At the surface, flood currents predominate over ebb currents in the northern part of the entrance, in North Channel, and in Chesapeake Channel. In the seaward opening channel between Inner Middle Ground and Nine Foot Shoal, on the average, the surface flood at strength is 93 cm/sec; whereas, the ebb at strength is 57 cm/sec. Surface ebb currents predominate over flood currents in the approaches to Thimble Shoal Channel, in the southern part of the entrance.

At the bottom, the pattern of ebb or flood dominance is somewhat altered. Flood currents are of greater duration at the bottom than at the surface and reach their local peak velocities sooner. Thus some stations that exhibit minor ebb dominance at the surface are shifted to flood dominance at the bottom. This is especially the case in the deep main channel in the southern part of the entrance. A provisional pattern of ebb-flood dominance for the entire entrance area at the bottom has been adduced by Ludwick (1970b).

At two specific locations, one in North Channel and the other atop a sand bank, water motion effective in moving local sediment is seen to be substantially different (Fig. 4). In North Channel, effective flood-directed motion exceeds effective ebb-directed motion; whereas, atop the bank, effective ebb-directed motion dominates.

The gross circulation of the estuary averaged over time is that of a moderately stratified estuary (Pritchard, 1967). Tidal currents reverse with ebb and flood at all depths in the entrance area; however, the mean flow is such that there is a net outflow of water in the surface layers as a whole and a net inflow of water in the bottom layers. The depth of the zone of no net motion is presently estimated to be between 5 and 7 m.

The geographic location of a fixed survey line was chosen with regard to achieving perpendicularity to the trend direction of the crests of sand waves as determined during previous surveys (Ludwick, 1970a). It was also intended that the line should be located in such a position that, if direction and magnitude of sand wave migration were detected, some new light might be shed on shoal construction processes, on the role of tidal currents acting in North Channel, the master channel of the northern entrance area, and on the effect of tidal currents on bank tops. The locations of the three points, A, B, and C, that define the fixed survey line are shown in Figure 3. The A-B distance is 2630 m; the B-C distance is 3619 m. Total line length is 6.2 km.

Each day, before the fixed line was occupied for the purpose of resurveying, eight buoys were set out along the line. Every effort was made to set a buoy exactly on point B. The other seven buoys were set on or very near to the line but not necessarily at predetermined places along the line. Average distance between buoys was 910 m, a distance that permitted the sighting of 1 to 4 buoys on the line ahead of the vessel. Average water depth along the line is approximately 7.6 m. A buoy tether line length of twice the water depth, or 15.2 m, was found satisfactory under most conditions of current. A set of four 3.6-kg. rod-shaped iron weights linked together comprised the anchor for each buoy. When the currents were especially strong, a set of 6 weights was used.

After a buoy was provisionally set, the bow of the survey vessel was brought up to the buoy and an observer on the bow, using a sextant, measured horizontal angles between three known landmarks such as lighthouses, bridge spans, and radio navigation towers. Immediate plotting of the position using a metal, precision 3-arm protractor showed whether the buoy location was sufficiently close to the survey line or not. If the distance between the plotted buoy location and the survey line was 10 m or more, the buoy was dragged closer to the line, and the new position determined as before. In practical, realistic tests, it was repeatedly shown that a point in the water could be reoccupied to within 10 m or less using the sextant method, the same instrument, the same observer, and the same sighting points. Buoys were often checked to determine whether dragging had occurred. If so, the run was rejected. If it so happened that the tide turned after the buoys were set but before the line was run, a correction was made to the chart position of each buoy.

Water depth along the line of buoys was recorded using an Edo Model 578 precision depth recorder aboard the survey vessel. The paper record is made on rectangular coordinates at a depth scale of 1 cm (recording chart) per 1.28 m water depth. Chart speed through the instrument is 5.08 cm/min which corresponds to a horizontal scale of 1 cm (recording chart) per 6.09 m ground distance at a ship speed of 10 knots. Frequency of the sounding signal is 80 kHz. The acoustic cone angle between half power points is 8 degrees. Draft adjustment, power supply frequency adjustment, and depth check were made prior to each run.

The line of buoys was followed by the survey vessel in making a run. Maximum use was made of multiple buoy sightings ahead of the ship. Compass heading was observed continuously and a run was not considered acceptable unless a constant angle of crab was maintained during a run. This last precaution insures that the ship does not drift systematically away from the fixed line between buoys due to cross currents. The strip chart was marked as each buoy was passed abeam. On each day of survey the line was run twice.

Sand Waves on Profile A-B-C

Although comparisons among runs of the profile taken at different times reveal substantial differences, there are gross features of the bathymetry along the line that are more or less unchanging. It is these gross aspects that are to be described in this section. The changes with time will be treated in a following section. Among the gross aspects of the profile, the most obvious is the presence of larger sand waves on the seaward half of the profile, in contrast to the presence of smaller sand waves on the landward half of the profile (Fig. 5). In the paragraphs below the larger features are first described.

The trough to crest height of the largest seaward sand waves averages 1.9 m. The measurement refers to the vertical distance between the crest and the trough that is situated immediately seaward. Water depth to the shoalest sand wave crest averages 5.0 m relative to MLW. Most of the sand waves on this part of the line are of approximately the same height. There is no definite indication of an increase in height with distance along the seawards part of the transect.

Wave length of the seaward sand waves was determined by means of spectral density analysis (Nordin and Algert, 1966; Nordin, 1968; Crickmore, 1970). The peak of the spectrum (Fig. 5) corresponds to a wave length of 274 m. The mean of the spectrum, an alternative characterization, is 211 m. To obtain the spectral analysis, the original record of the run for December 29, 1969, was digitized at record intervals of 0.847 mm. Water depth was measured relative to MLW. In calculating ground distance, adjustments were made for slight differences in speed of the survey vessel between each pair of buoys along the survey line.

Overall slope of the bottom along the whole line interferes with spectral analysis. A filtering procedure designed for slope removal was performed by taking a 101-point moving average of the water depths. In a final profile, elevations were calculated for each point relative to this mean surface. The resulting data set is characterized by a mean of zero. Elevations are standardized by setting the maximum deviation from the mean surface equal to unity, and changing all other values in the data set proprotionally. The actual spectrum was obtained using the fast Fourier transform method embodied in a computer program written by my colleague, Dr. W. D. Stanley.

The asymmetry of the seaward sand waves is pronounced. Long gentle slopes on the backs of the features are inclined landwards; whereas, shorter, steeper slopes forming the forefronts of the features are inclined seawards. Backslopes average less than one degree; steeper forefront slopes average 1.5 degrees and occasionally reach 6 degrees.

In contrast with the foregoing features, the sand waves on the landwards part of the profile are smaller and shorter. The average trough to crest height of the largest waves in this group is 1.4 m. Water depth to the crests of the shoalest sand wave averages 5.2 m below MLW. There is a rather strong indication that the height of the waves decreases with distance from B towards C, but the amount of decrease is less than 0.5 m. Sand waves essentially die out on the inner 0.5 km of the transect except for a single feature near the inshore end of the line.

Wave length of the inner sand waves was also determined by means of spectral analysis (Fig. 5). The peak of the spectrum indicates that maximum power is contained in a sinusoidal component whose wave length is 86 m. The mean of the spectrum is 93 m. The principal component dominates over other nearby frequencies to a greater extent than is the case for the peak frequency in the seawards part of the profile. The inner sand waves are more regular in spacing and height and better fitted by a single sine wave than are the larger sand waves present on the outer part of the line.

The profile form of the inner waves is asymmetrical-trochoidal in contrast to the asymmetrical form of the outer sand waves. A few of the inner waves occasionally approach a perfectly symmetrical trochoidal form. When this is the case for a wave, both seawards and landwards slopes are concave upward, and the crest is quite peaked. This aspect of the features is emphasized by the vertical exaggeration in the field record, but nevertheless when allowance is made for this distortion, the slopes near pointed tops are seen to approach the angle of repose of the sediment. Most of the time. and over most of the profile, slopes of the inner sand waves are well below the angle of repose, as is also the case with the larger outer sand waves.

The contrast in sand wave length, asymmetry, and height between the outer part of the whole profile and the inner part of the whole profile is marked. The line of division between the two sections is not sharp, but it appears to be located between 900 and 1000 m west of point E on the profile (Fig. 5). When the position of this zone of division is transferred to the transect profile obtained after smoothing, it is seen that the inner sand waves lie on one side of the high point, or divide, and that the outer larger sand waves lie on the other side of that point on the profile. The high point, or divide, separates North Channel from the unnamed channel to the south (Fig. 3). There is apparently some difference in near-bottom tidal current regimes on either side of the divide.

Small Scale Features of the Sand Waves

Certain small scale features of the sand waves are sufficiently common among the set of sequential profiles to warrant description. These features include the catback profile, the foreslope step and hole, and some very small order features discernable on the profile traces.

The term catback was first used by Van Veen (1935) to describe some unique profiles of sand waves surmounting the great tidal sand ridges of the North Sea. The term denotes a profile humped at one end and terminated at the other end by a small higher pointed peak from which the bottom drops off abruptly into deeper water. Features of this form are common to both inner and outer sections of the present profiles (Figs. 6A1, 6D1, 6F1). The surmounting peak often rises 0.7 m or so above the top of a sand wave. Peaks occur at the top of the foreslope of an asymmetrical sand wave, or in the center of a wave profile, or on the forefront slope itself. Presence of the features in identical positions on repeated profiles indicates that the peaks are not spurious records due to surface water wave motion.

On the foreslopes of asymmetrical sand waves occasionally there are step-like features that interrupt the slope as it descends into the trough (Figs. 6B1, 6B2, 6E1, 6E2). The more or less horizontal surface of a step is approximately 150 m in width. The drop at the edge of this surface is approximately 0.6 m, beyond which the foreslope continues downwards into the trough. The edge of the step often bears a small peak. There are some instances in which the trough beyond a step appears to be abnormally deep, with steep sides so that the trough itself appears as a hole or notch in the profile (Figs. 6B1, 6B2, 6B3, 6E1, 6E2, 6F1). Troughs between waves of the outer profile section are often complex in form (Figs. 6E1, 6E2). They are the site of holes, compound smaller waves surmounted by small peaks, multiple steps, small sharply asymmetrical dune-like forms, undulations, and other features. Some waves of the outer profile, particularly those that are not strongly asymmetrical, display steps on both seaward and landward sides (Figs. 6C1, 6C2, 6C3, 6C4).

It is quite possible to separate waviform bottom features on the echo-sounding record from oscillations due to surface water wave motion if the apparent periods of the two are substantially different. At an acoustic cone angle of 8 degrees and a water depth of 6 m, a bottom area 0.8 m across is insonified. At a ship speed of 10 knots, this distance corresponds to a record length of 1.4 mm, or 1.65 sec. Thus features 0.8 m in wave length on the bottom can be distinguished from the average surface water wave motion which has a period of 5 sec. When the ship moves in the direction of surface water wave propagation, as was usually the case, the effective period of the surface waves becomes 15 sec, and small features on the bottom are even less confounded.

It is evident that much of the profile commonly bears small waviform features on its surface (Figs. 6E1, 6E2, 6F1). These irregularities are approximately 10 m in wave length and 0.3 m in height and may be small sand waves or dunes. Direct observation by divers will ultimately resolve this issue. The features are often strongly asymmetrical in profile. A common occurrence shows small features on one face of a large sand wave and an absence of similar small features on the other face which is usually the steeper side of the sand wave (Figs. 6B2, 6F1). Another occurrence shows small asymmetrical features on both sides of a larger sand wave (Figs. 6C1, 6E2). In this instance, the small features on both sides commonly face upslope in the direction of shoaling.

Bottom sediment along the profile is medium-grained sand. Coarsest quartz grains in each of 15 samples taken from the profile range from 3 to 7 mm in diameter with no systematic variation along the profile. The weight of sediment finer grained than 0.062 mm ranges from 1.7 to 0.7 percent among the samples. Most of the samples contain 10 percent of coarse-grained broken worn shell fragments. Both the shell fragments and coarse quartz particles are iron-stained giving the samples a brownish coloration.

Changes in Sand Waves on Profile A-B-C

The most obvious change with time in the sand waves on profile A-B-C is in the height of the features. Among the 21 successive profiles, 5 show the bottom undulations to be low in relief, rounded in profile form particularly at sand wave crests, and free of irregularities along the surface. In contrast, 8 profiles show the bed waves to be high in relief, sharp and peaked particularly at sand wave crests, and frequently marked with sharp irregularities on foreslopes and in troughs. Steepest slopes found anywhere in the whole ensemble occur in this set. Some of the slopes among the forms in the group are as steep as 24 degrees. These steep slopes are usually near the tops of sand waves and occur on the seaward side of the outer asymmetrical forms. On the inner asymmetrical-trochoidal features, the steep angle of repose slopes comprise the aforementioned sharp trochoidal peaks (Fig. 6A1).

Survey dates of records in the low rounded class, denoted by half-circles in Figure 7, and dates of records in the high peaked class, denoted by triangles, are entered in the time-series plots of tidal height, tidal current strength, tidal current dominance, and wave or swell height (Fig. 7). It is readily seen that there is no correlation of the two classes with the tidal data. There is a strong correlation of the classes with the wave and swell data. Dates of the low rounded records correspond to that period of several months duration in which there are frequent episodes of high surface water waves or swells. Dates of the high peaked records correspond to those periods during which there are infrequent episodes of high surface water waves or swells. A surface water wave height of 1.5 m (5 ft) appears to be the value that best separates high waves or swells from low waves or swells and hence low records from peaked records. The actual statistic plotted in the time-series diagram is the average, for each day, of eight 3-hourly observations of wave height and swell height. For each of the 3-hourly observations, used in computing the average, either wave height or swell height is used depending on which is larger.

An analysis of the dates of the low rounded group of profiles shows that, with one exception, they occur between October 6, 1969, and December 29, 1969. The one possible exception occurred on April 25, 1969, a date prior to which there is no continuous analyzed record of wave and swell heights for examination. The most characteristic member of the group is the record for November 8, 1969. Sand waves are lower and more rounded on this record than on any other. Examination of Figure 7 shows that October 6, 1969, marks the first survey made following a 5-day period of unusually high waves and swells. No peaked, and hence contradictory, records were obtained during the period from the beginning of October to the end of December. It seems very likely that the period of low rounded profile types extends beyond December perhaps until late April, but no records were taken during this period owing to unavailability of the survey ship.

Dates of records of the high peaked type range from June 12, 1969, to September 12, 1969. In 1970, records of this same type were obtained on May 12 and on September 9. Thus it would appear that this type of record occurs from May to September, a period of 5 months. There is an indication that records obtained in May and June, although showing high peaked sand wave types, are not extreme; whereas, records taken later on in September show the maximum development of high peaked forms. This latter month shows very few occurrences of surface water waves or swell height greater than 1.5 m.

The magnitude of the change in sand wave height during the year is considerable. First, with reference only to the seaward part of the profile, and with reference only to highest sand waves on each of the records, the height ranges from a minimum of 1.46 m to a maximum of 2.50 m, an increase of 71 percent. Second, with reference only to the landward part of the profile, and again with reference only to the highest waves on each of the records, the height ranges from a minimum of 0.92 m to a maximum of 2.13 m, an increase of 232 percent. The landward sand waves which are asymmetrical-trochoidal in profile undergo more than a seasonal doubling in height during the year and experience a greater change in height than do the seaward sand waves which are asymmetrical in profile.

A question that is closely related to change in sand wave height is whether an increase in height is due only to a build-up of the crest, or whether an increase in height is due only to a deepening of the trough, or whether the observed increase in height is due to both crest build-up and trough deepening. Examination of the data from the profiles indicates that both crest build-up and trough deepening occur when the height increases. Relative to MLW no sand wave was observed with less than 4 m of water atop its crest.

In addition to changes in sand wave profile and height with time, there are also significant changes in sand wave position during the 17-month observation period. It was found possible to identify corresponding sand waves from record to record with essentially no uncertainty despite one time gap of four months. The average time gap between successive surveys was 24 days. Slowness of sand wave migration relative to elapsed time between surveys is what makes crest matching certain and error free. The time-position history of 36 different sand wave crests or troughs was followed during the total period of study.

Migration rates of sand waves on the profile were determined from plots of crest, or trough, position against time, so-called travel-time plots (Fig. 8). The slope of the best fit travel-time line is equal to the migration speed of a sand wave under study. Preliminary examination of the travel-time plots revealed that there was an irregular linear trend to the travel-time curves, and for this reason linear regression analysis was used to fit straight lines to the observed data. Linear regression analysis, as is well-known (Sokal and Rohlf, 1969), assumes that one of the arguments, either time or position in this study, is error free. Since the date of each successive survey was known, this argument was taken to be error free, and hence is taken as the independent variable. Position of a sand wave was taken as the dependent variable. Thus the line of fit that was obtained in each instance was the regression of sand wave position on time.

The relevant statistic obtained from the regression analysis is the regression coefficient, which is the slope of the line of regression of sand wave position on time. A regression coefficient, or slope, was obtained by the conventional least squares method for each of the 36 sand waves studied. The units of the regression coefficient are length per time. It was convenient to choose meters per year to express sand wave migration rate.

Examination of Tables I and II reveals that the maximum sand wave travel rate was 150 m/yr. The direction of travel was seawards. The sand wave involved in this motion was situated at the extreme seawards end of the profile. The rate may be somewhat in doubt because only four successive runs were available for this feature. It exited beyond point A on subsequent runs. The other extreme sand wave migration rate observed was 15 m/yr (Table II). For this wave the direction of travel was landwards. This wave is in the landwards section of the transect where the bottom features are asymmetrical-trochoidal in profile form. This wave is one of two on the entire transect that showed a landwards direction of travel. The average of all the 36 migration rates is 40.2 m/yr, and the direction is seawards.

It is seen in Tables I and II that sand wave travel rates differ between the landwards and seawards sections of the transect. Landwards of a point approximately 760 m west of point B on the transect, most sand wave migration rates are less than 34.8 m/yr; whereas, seawards of that division, travel rates are greater than 34.8 m/yr. If valid, average migration rate of sand waves on the landward segment would be 22.2 m/yr; whereas, average migration rate of sand waves on the seawards segment of the transect is 63.1 m/yr, or nearly three times as great. Direction of sand wave migration is seawards in both segments.

The question naturally arises as to whether there were a sufficient number of successive observations of the sand waves to warrant acceptance of the calculated migration rates. A significance test for regression coefficients as given by Sokal and Rohlf (p. 420) was used to answer this question. In the present instance, the calculated regression coefficient was tested against a regression coefficient of zero, i.e., zero migration rate. The significance test indicates the probability that an observed difference in regression coefficient from zero would occur by chance alone.

With reference only to the 16 features on the seaward segment of the transect (Table I), 8 of the regression coefficients obtained were significant at the 0.05 level or better; 14 were significant at the 0.20 level or better. That is to say that there is only a 5 percent probability, or less, that a regression coefficient as large as that obtained would occur by chance alone if the true regression coefficient were actually zero. At least one-half the calculated migration rates, and perhaps all but two, are deemed significant. It is concluded that the large outer asymmetrical sand waves are actually migrating. Those closest to point B yielded the least acceptable significance tests.

With reference only to 20 features on the landward segment of the transect (Table II), 16 of the regression coefficients obtained were considered not to be significantly different than zero, the test yielding values of 0.40 or larger. This figure indicates that 40 percent of the time one would expect to obtain regression coefficients as large as those obtained if the true regression coefficient were actually zero. It is concluded that symmetrical-trochoidal sand waves found on the landwards part of the transect are not migrating, at least not within detectable limits of the experiment.

For those large asymmetrical sand waves that were found to migrate significantly, 95 percent confidence limits were calculated for the migration rate. It is seen in Tables I and II that the statistically justifiable conclusion is that these waves migrate at rates greater than, say, 15 m/yr but less than, say, 100 m/yr.

Detailed examination of the travel-time curves indicates the existence of some instances in which sand waves appear to move oppositely to their long term seaward motion. Some of these instances are supported by several successive surveys, each of which shows a retrograde motion. The fact that not all the sand waves are affected at the same time lends credence to actual retrograde motion rather than an explanation based on positioning error. An example is shown in Figure 8, sand wave number 5, late August and September.

The fluid environment of the sand wave area is comprised of many factors all of which vary with time. In Figure 7 the variation during the 17-month observation period has been shown for tidal height, tidal currents, fresh water run-off, wind speed, and wave or swell height. As regards tidal height, for each day the forecasted higher high water and lower low water elevations were obtained from tide tables for a point near the transect. As regards tidal range, for each day the larger range from high water to following low water was plotted. Synodic variations dominate the plot. As regards tidal currents, a plot is presented for the shoal top (Station 9, Fig. 3) of the variation in maximum forecasted ebb velocity at the water surface and maximum forecasted flood velocity at the water surface. There is a strong correlation between tidal range and tidal current speed. A plot is also presented of the difference, or residual, of ebb and flood tidal currents. Surface ebb currents are dominant at Station 9 on a time basis during the 17 months and also in the magnitude of the residual velocity. Data are also plotted for the sum of the fresh water discharges of gauged rivers that enter Chesapeake Bay. Destructive flooding in the Appalachian Mountains following the rains from hurricane Camille are evidenced in August, 1969. Also shown is wind speed at a light tower station off the entrance to Chesapeake Bay. Individual data points are daily averages of eight 3-hour observations. The wave height or swell height data have been described in a previous paragraph. Finally, surface salinity is given for the entrance area.

Discussion

The finding, in this study, of large migrating tidal sand waves whose slopes are everywhere substantially less than the angle of repose of the constituent sediment, requires an explanation different from that usually given for the mechanism of sand wave movement under unidirectional flow. With backslopes and foreslopes of 1 degree, or thereabouts, and at near-bottom flow rates less than 1 m/sec, significant boundary layer separation at a sand wave crest is unlikely, there is no lee eddy, there is no avalanche slope, and hence the usual mechanism of sand wave advance by the continued forward building of avalanche faces is infrequent or non-existent.

By prior usage, these low-slope forms would be termed para-ripples (Bucher, 1919) if symmetrical or nearly symmetrical and lacking grain assortment. They would be termed accretion ripples (Imbrie and Buchanan, 1965) if asymmetrical in profile form, the term, accretion, being taken from Bagnold's (1941) term, accretion deposit, which denoted gently sloping, curved, tapering aeolian cross-strata lacking conspicuous grain assortment. Although the last pair of authors did not observe the actual formation or movement of accretion ripples in their study of Bahamian deposits, they concluded from other evidence that accretion deposits with set thicknesses of 2.5 to 15.0 cm are formed by high velocity currents at least one-half meter thick moving down the lee side of an accretion ripple or other migrating embankment. They reasoned that accretion deposits, and hence accretion ripples, were formed at current speeds greater than those required to form avalanche faces but still in the lower flow regime. In the following paragraphs an alternative mechanism is presented for the migration of low-slope sand waves under reversing unequal tidal flow at velocities substantially less than F = 1.

Near-bottom critical erosion velocity varies with bed slope (White, 1940; Vanoni et at., 1966), a lower downslope flow velocity being required to initiate sediment motion on a sloping bed than on a horizontal bed because the downslope component of gravity aids entrainment. The form of the relationship is

$$V_c = K_1 \, (\tan \alpha \cos \theta - \sin \theta)^{\frac{1}{2}},$$

where V_c is the critical flow velocity for initiation of sediment motion and is measured near the bed; K_1 is a dimensional constant that includes the effects of particle size, shape, and density as well as fluid density; α is the under-water angle of repose of the sediment; and θ is the slope of the bed measured positively downward from horizontal in the direction of fluid flow.

As seen earlier in this paper, small bedform migration speed when related solely to fluid flow velocity, is not unreasonably given in the form,

$$c_r = K_2 \, (V - V_c)^n \, , \quad V \geqq V_c$$

where c_r is bedform migration speed, K_2 is an empirical constant and depends on the choice of measurement units, V is the fluid flow velocity measured near the bottom, V_c is the critical pick-up velocity as in the preceding equation, and n is an empirically determined constant that appears to depend on size of the bedforms, particle size, and probably other factors.

If the previous expression for V_c is substituted in the equation above, small beform migration speed, c_r, is then given in the resulting equation as a function, primarily, of bed slope and near-bed fluid flow velocity. Consistent calculation of bedform migration speed on beds of different slope can be made if the various constants are assigned reasonable values. In the analysis that follows, α is taken as 30 degrees, K_1 is taken as 0.4, which value gives V_c an acceptable magnitude in meters per second when $\theta = 0$ degrees, K_2 is taken as 200, which when coupled with $n = 2.5$ gives a relationship between bedform migration in meters per day and fluid velocity in meters per second not unlike those of other workers (Fig. 1).

Now under tidal flow of known or assumed velocity near the bed, the equation can be used to estimate small bedform migration speed. To model sediment transport conditions on sand waves similar to those found on the subject survey transect, it is further assumed that near-bottom ebb velocity, V_e, is constant and greater than near-bottom flood velocity, V_f. Duration of ebb and duration of flood are each taken as 6 hours. Model sand waves for the area have a wave length of 200 meters and foreslopes and backslopes are equally inclined at 1 degree from the horizontal. For purposes of analysis, foreslopes and backslopes are divided into serially numbered cells, each of which is 5 meters in length.

The results of a sample computation using the equation described above are illustrated in Figure 9, where V_e is assumed to be 0.42 m/sec and V_f is assumed to be 0.41 m/sec. Residual migration is seaward on both slopes. This situation obtains if ebb flow velocity exceeds flood flow velocity by more than 0.009 m/sec.

Under ebb flow, small bedforms that have been moving rapidly downslope are slowed when an upslope is met. This slowing-down by itself would be expected to produce a contraction in crest-to-crest bedform spacing of the small bedforms on the upslope. This is tantamount to an increase in sediment thickness per unit length of upslope as compared to the thickness of moving sediment per unit length of downslope. Bumper-to-bumper automobile traffic occasioned by slow passage through a tunnel is an analogy. The ratio of the number of bedform crests per unit length of upslope to the number of bedform crests per unit length of downslope is given by c_{red}/ c_{reu}, where the numerator is bedform migration rate on ebb flow on a downslope, and the denominator is bedform migration rate on ebb flow on an upslope. Under flood flow, the relative increase in sediment thickness on an upslope is correspondingly given by c_{rfd}/ c_{rfu}.

It is inferred from the foregoing that the slowing-down of bedform migration rate on adverse slopes is responsible for the development of sediment steps seen on the sand wave profiles that were described and figured earlier in this paper. Steps were found on both foreslopes and on backslopes of sand waves giving the waves a "head-and-shoulders" appearance. The common complexity of the bottom seen in troughs between large sand waves is thought to be due to the change in bedform migration rate at that place, both on ebb and flood flows.

At the top of the large sand waves where the slope of the bottom is more or less level, the ebb-dominated tidal flow causes a net seawards sediment motion which, over time, fills the pocket on the seaward side of the feature between the crest and the seaward step. By these mechanisms, the large sand waves are believed to migrate seaward.

The explanation given above singles out small migrating bedforms as the main causal agent for movement of the large bedforms; however, observations by scuba divers have shown that there is, in addition to the small bedforms, a cloud three feet thick, or thereabouts, of moving sediment and water in contact with the bed when tidal currents are flowing. This moving sediment probably also plays an important role in migration processes of the large sand waves. The equation presented above can be used to explore consequences of such movement by assigning a larger magnitude to the constant, K_2. This alteration allows for the much greater mobility of the sediment-water cloud as compared to small migrating bedforms and yet maintains the effects of upslopes and downslopes on speed of sediment motion.

Trajectories of particles for one ebb-flood cycle under different ebb and flood velocities were examined using the equation. One sediment particle was positioned initially in each cell of the model sand wave referred to above. The initial departure of a particle from a cell was denoted by the symbol, -1. The coming-to-rest of a particle in a cell at the end of one ebb-flood cycle was denoted by the symbol, +1. The algebraic sum of the losses and gains in each cell after one ebb-flood cycle indicates the net accumulation or net removal of sediment from that cell. Trajectories that begin on adjacent sand waves affect the outcome on a central sand wave to which interest was principally directed.

Results obtained indicate that for most reasonable combinations of ebb and flood velocities there is an accumulation of sediment on seaward-facing slopes and in troughs between sand waves. Minor erosion or zero net change occurs in cells positioned elsewhere along the sand wave profile.

The migration rates of the larger seaward sand waves, as well as the travel rates of the inner asymmetrical-trochoidal sand waves, are slow compared to the probable movement rates of sediment ripples and the even faster translation rates of the cloud of moving sediment and water near the bottom. This disparity in relative travel rate requires the existence in the bed of a traction layer at least 30 cm thick. It seems likely that there is net sediment transit through the sand wave field in this upper surface zone. In this sense the large sand waves may be likened to the kinematic waves described by cloud meteorologists, traffic engineers, and queuing theory mathematicians. These kinematic waves, either stationary or moving, result from local bunching-up of particles, or automobiles, or unit parcels due to a change in forward velocity of the units. Nevertheless, the units pass through the waves. It would appear that considerable development and extension of this analogy should be possible.

The migration and profile form of the sand waves on profile A-B-C shed some new light on the configuration of ebb-dominated and flood-dominated tidal flows in the sand bank area of Chesapeake Bay entrance. Judged from findings presented above, the unnamed shoal on which profile A-B-C is situated (Fig. 3) is an embryonic flood parabola, in the usage of Van Veen (1936, 1950), i.e., a parabolic-shaped shoal open to flood tidal currents. The seaward-facing asymmetrical, faster-moving sand waves of limb A-B and part of B-C are apparently located on the flank of what Hayes (1969) has termed an ebb spit. This is a long trailing tail of a flood parabola (Fig. 10). This section is exposed to ebb currents which are quite strong because of the convergence of channel margins. Flood currents in this position outside the limbs of the parabola are much weaker than the ebb currents.

Limb B-C is chiefly through smaller asymmetrical-trochoidal sand waves that also face seawards. These waves apparently owe their more symmetric form and low migration rate to flood currents which somewhat offset the oppositely directed powerful ebb currents. The ebb currents are not as strong in this section as in section A-B because there is much less channel constriction. The flood currents are stronger over this section (B-C) as is consistently the case for flow between horns of flood parabolas. Nevertheless, as shown in Figure 4, ebb-directed currents still exceed flood-directed currents.

The sand bank area in the entrance to Chesapeake Bay is contiguous with the sand ridge and swale bathymetry of the continental shelf off the eastern United States (Uchupi, 1968). The question of the origin of that bathymetry is not markedly clarified by the present study because the tidal currents insofar as they are known are so appreciably different in strength between the two areas. Findings of the present study relate chiefly to shoaling in tidal entrances or to areas like Nantucket Shoals or Georges Bank where bottom currents are strong enough to move substantial quantities of sand-sized sediment.

Conclusions

The following are the principal conclusions reached in this study:

1. In close proximity, on a shoal in the tidal entrance to Chesapeake Bay, there are large asymmetrical seaward-facing sand waves and smaller asymmetrical-trochoidal seaward-facing sand waves. The large features are approximately 270 m in wave length and 1.9 m in average height. The smaller features are 85 m in wave length and 1.4 m in height. Both waves lack avalanche slopes; the average slope is 1 degree or less but slopes up to 6 degrees occur occasionally and in the extreme reach 20 degrees.

2. The asymmetrical-trochoidal waves occur on one side of a bathymetric divide atop a shoal; the asymmetrical sand waves occur on the other side of the divide.

3. Profiles of the sand waves display catback shapes, sediment steps on one side or on both sides of central sand waves, and holes or other irregularities, especially in troughs between sand waves. Small sand waves, 10 m in length, 0.3 m in height, display avalanche slopes and commonly face upslope on both sides of large sand waves.

4. A survey line across the aforementioned features was surveyed 22 times over a 17 month period. The large asymmetrical sand waves migrate seawards at rates between 15 and 100 m/yr and average 63 m/yr. These rates were shown to be significant statistically. The smaller asymmetrical-trochoidal sand waves could not be shown to be migrating within the detection limits of the experiment.

5. The sand waves studied were shown to be located on the margin of what is probably a flood parabola (Van Veen, 1936); the large asymmetrical sand waves were on the ebb-dominated flank of the ebb spit (Hayes, 1969); the small asymmetrical-trochoidal sand waves were on the ebb-dominated shoal top but so situated as to be subject to strong flood flow emanating from a flood-dominated channel between the horns of the flood parabola.

6. The low-slope sand waves lack avalanche slopes and are believed to migrate under the existing subcritical flow conditions by the construction of sediment steps or secondary waves on sand wave flanks. These steps or secondary waves represent accumulations due to upslope slowing down of small migrating bedforms. Sediment transport on sand wave crests, by small migrating bedforms, fills the pocket between the crest and the step or secondary sand wave. Under ebb-dominated flow, this filling occurs more rapidly on the ebb side than on the flood side of the wave, thereby causing an apparent ebb migration of the entire large wave.

7. Sand waves were seen to undergo a pronounced seasonal change in profile form. From May to September, profiles showed relatively steepened, higher, peaked forms; whereas, from October to April, profiles showed lower rounded forms for the same sand waves. The apparent cause is the near absence of surface water waves or swell higher than 1.5 m from May to September; whereas, surface water waves and swell higher than 1.5 m occur frequently from October through April.

REFERENCES

Allen, J. R. L., 1962. Asymmetrical ripple marks and the origin of cross-stratification. Nature, 194: 167-169.

Allen, J. R. L., 1963. Asymmetrical ripple marks and the origin of water-laid cosets of cross-strata. Liverpool Manchester Geol. J., 3: 187-236.

Allen, J. R. L., 1965. Sedimentation to the lee of small underwater sand waves. J. Geol., 73: 95-116.

Anonymous, 1967. The northern limit of megaripples in the North Sea. Hydrographic Newsletter, 1: 339-340.

Ashida, K. and Tanaka, Y., 1967. A statistical study of sand waves. Proc. XIIth Internat. Assoc. Hydraulic Res., 2: 103-110.

Bagnold, R. A., 1941. The Physics of Blown Sands and Desert Dunes. Methuen, London, 165 pp.

Ballade, P., 1953. Etudes des fonds sableux en Loire Maritime, nature et evolution des ridens. Comité d'Oceanographic Bulletin d' Information, 5: 163-176.

Belderson, R. H. and Stride, A. H., 1966. Tidal current fashioning of a basal bed. Marine Geol., 4: 237-257.

Bucher, W. H., 1919. On ripples and related sedimentary surface forms and their paleographic interpretation. Am. J. Sci., 47: 149-210, 241-269.

Carey, W. C. and Keller, M. D., 1957. Systematic changes in the beds of alluvial rivers. Proc. Am. Soc. Civil Engrs., 83(HY4): 1-24.

Cartwright, D. E., 1959. On submarine sand-waves and tidal lee-waves. Proc. Roy. Soc. (London), Series A, 253: 218-241.

Chang, Y. L., 1939. Laboratory investigation of flume traction and transportation. Trans. Am. Soc. Civil Engrs., 104: 1246-1284.

Cloet, R. L., 1954 a. Sandwaves in the southern North Sea and in the Persian Gulf. J. Inst. Navig., 7: 272-279.

Cloet, R. L., 1954 b. Hydrographic analysis of the Goodwin Sands and the Brake Bank. Geogr. J., 120: 203-215.

Cornish, V., 1901. On sand waves in tidal currents. Geogr. J. London, 18: 170-202.

Crickmore, M. J., 1970. Effect of flume width on bed form characteristics. Proc. Am. Soc. Civil Engrs., J. Hydraulics Div., 96(HY2): 473-496.

Deacon, G. F., 1894. Discussion of "Estuaries" by H. L. Partiot. Proc. Inst. of Civil Engrs., 118: 47-189.

Dingle, R. V., 1965. Sand waves in the North Sea mapped by continuous reflection profiling. Marine Geol., 3: 391-400.

Forel, F. A., 1883. Les rides de fond etudiées dan le Lac Leman. Archives des Sciences Physiques et Naturelles, 3 Sér., 10: 39-72.

Gilbert, G. K., 1914. The transportation of debris by running water. U.S. Geol. Surv., Profess. Paper, 86: 1-263.

Harms, J. C., 1969. Hydraulic significance of some sand ripples. Geol. Soc. Am. Bull., 80: 363-396.

Harvey, J. G., 1966. Large sand waves in the Irish Sea. Marine Geol., 4: 49-55.

Hayes, M. O., 1969. Forms of accumulation in estuaries. In: Coastal Environments of Northeastern Massachusetts and New Hampshire - Coastal Research Group, Contribution No. 1-CRG, Geology Dept., Univ. of Mass., Amherst, Mass., 462 pp.

Houbolt, J. J. H. C., 1968. Recent sediments in the southern bight of the North Sea. Geologie en Mijnbouw, 47 (4): 245-273.

Imbrie, J. and Buchanan, H., 1965. Sedimentary structures in modern carbonate sands of the Bahamas. In: G. V. Middleton (Editor), Primary Sedimentary Structures and Their Hydrodynamic Significance - Soc. Econ. Paleotologists and Mineralogists, Spec. Publ., 12: 149-172.

James, N. P. and Stanley, D. J., 1968. Sable Island Bank off Nova Scotia: sediment dispersal and recent history. Am. Assoc. Pet. Geol. Bull., 52: 2208-2230.

Jones, N. S., Kain, J. M., and Stride, A. H., 1965. The movement of sand waves on Warts Bank, Isle of Man. Marine Geol., 3: 329-336.

Jopling, A. V., 1965. Laboratory study of the distribution of grain sizes in cross-bedded deposits. In: G. V. Middleton (Editor), Primary Sedimentary Structures and Their Hydrodynamic Significance - Soc. Econ. Paleotologists and Mineralogists, Spec. Publ., 12: 34-52.

Jordan, G. F., 1962. Large submarine sand waves. Science, 136: 839-848.

Kennedy, J. F., 1963. The mechanics of dunes and antidunes in erodible-bed channels. J. Fluid Mech., 16(4): 521-544.

Kennedy, J. F., 1969. The formation of sediment ripples, dunes, and antidunes. Annual Review of Fluid Mechanics, W. R. Sears, Editor, 1: 147-168.

Kenyon, N. H. and Stride, A. H., 1968. The crest length and sinuosity of some marine sand waves. J. Sediment. Petrology, 38: 255-259.

Klein, G. de V., 1970. Depositional and dispersal dynamics of intertidal sand bars. J. Sediment. Petrology, 40: 1095-1127.

Lane, E. W. and Eden, E. W., 1940. Sand waves in the Lower Mississippi River. J. Western Soc. Engr., 45: 281-291.

Langeraar, W., 1966. Sand waves in the North Sea. Hydrographic Newsletter, 1: 243-246.

Leliavsky, S., 1955. An Introduction to Fluvial Hydraulics. Constable, London, 257 pp.

Ludwick, J. C., 1970 a. Sand waves in the tidal entrance to Chesapeake Bay: preliminary observations. Chesapeake Science, 11: 98-110.

Ludwick, J. C., 1970 b. Sand waves and tidal channels in the entrance to Chesapeake Bay. Virginia J. Sci., 21: 178-184.

Nordin, C. F., 1968. Statistical Properties of Dune Profiles. Ph. D. Dissertation, Colorado State University, Ft. Collins, Colorado, 137 pp.

Nordin, C. F. and Algert, J. H., 1966. Spectral analysis of sand waves. Proc. Am. Soc. Civil Engrs., J. Hydraulics Div., 92(HY5): 95-114.

Pritchard, D. W., 1967. Observations of circulation in coastal plain estuaries. In: G. H. Lauff (Editor), Estuaries, Am. Assoc. Adv. Sci., Publ., 83: 37-51.

Salsman, G. G., Tolbert, W. H., and Villars, R. G., 1966. Sand-ridge migration in St. Andrew Bay, Florida. Marine Geol., 4: 11-19.

Simons, D. B. and Richardson, E. V., 1960. Resistance to flow in alluvial channels. Proc. Am. Soc. Civil Engrs., J. Hydraulics Div., 86(HY5): 73-99.

Simons, D. B. and Richardson, E. V., 1961. Forms of bed roughness in alluvial channels. Proc. Am. Soc. Civil Engrs., J. Hydraulics Div., 87(HY3): 87-105.

Simons, D. B., Richardson, E. V., and Nordin, C. F., Jr., 1965. Sedimentary structures generated by flow in alluvial channels. In: G. V. Middleton (Editor), Primary Sedimentary Structures and Their Hydrodynamic Significance - Soc. Econ. Paleotologists and Mineralogists, Spec. Publ., 12: 34-52.

Smith, J. D., 1968. The Dynamics of Sand Waves and Sand Ridges. Ph. D. Dissertation, The University of Chicago, Chicago, Illinois, 78 pp.

Smith, J. D., 1969. Geomorphology of a sand ridge. J. Geol., 77: 39-55.

Sokal, R. R. and Rohlf, F. J., 1969. Biometry. Freeman, San Francisco, 776 pp.

Stride, A. H., 1963. Current-swept sea floors near the southern half of Great Britain. Quart.J. Geol. Soc. London, 119: 175-199.

Stride, A. H. and Cartwright, D. E., 1958. Sand transport at southern end of the North Sea. Dock and Harbour Authority, 39: 323-324.

Terwindt, J. H. J., 1971. Sand waves in the southern bight of the North Sea. Marine Geol., 10: 51-67.

Uchupi, E., 1968. Atlantic continental shelf and slope of the United States - Physiography. U.S. Geol. Survey Prof. Paper 529-C, 30 pp.

Vanoni, V. A., 1966. Sediment transportation mechanics: initiation of motion (Progress Report of Task Committee). Proc. Am. Soc. Civil Engrs., J. Hydraulics Div., 92(HY2): 291-314.

Van Straaten, L. M. J. U., 1950. Giant ripples in tidal channels. Konikl. Ned. Aadr. Gen. Tijdschr., 67: 336-341.

Van Straaten, L. M. J. U., 1953. Megaripples in the Dutch Wadden Sea and in the Basin of Arachon (France). Geologie en Mijnbouw, 15: 1-11.

Van Veen, J., 1935. Sand waves in the North Sea. Hydrographic Review, 12: 21-29.

Van Veen, J., 1936. Onderzoekingen in de Hoofden in verband met de gesteldheid der Nederlandsche kust. Ph. D. Dissertation, Leiden University, Netherlands, 252 pp., Printed at the Hague.

Van Veen, J., 1950. Ebb- and flood-channel systems in the Dutch tidal waters. Tidjdschr. Koninkl. Ned. Aardrijkskundig Genootschap, 67: 303-325. A.T.S. Translation 132 DU.

Visher, G. S., 1965. Fluvial processes as interpreted from ancient and recent fluvial deposits. In: G. V. Middleton (Editor), Primary Sedimentary Structures and Their Hydrodynamic Significance - Soc. Econ. Paleotologists and Mineralogists, Spec. Publ., 12: 116-132.

White, C. M., 1940. The equilibruim of grains on the bed of a stream. Proc. Roy. Soc. (London), Series A, 174: 322-338.

Figure 1. - Various proposed relations between the migration rate of undulose bed forms and unidirectional fluid flow velocity. Note the differences in size of feature, water depth, and definition of velocity used.

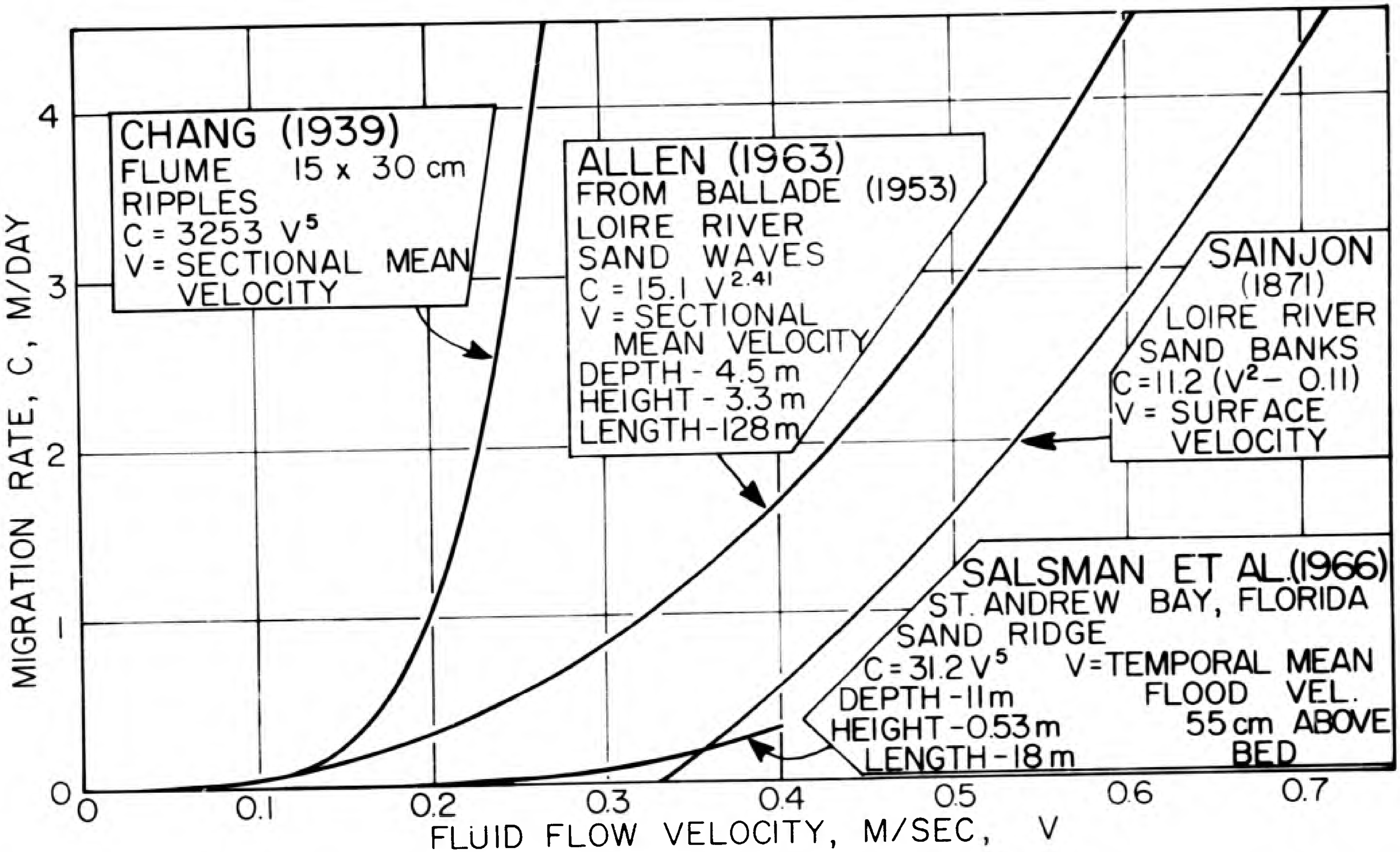
CHANG (1939)
FLUME 15 x 30 cm
RIPPLES
C = 3253 V^5
V = SECTIONAL MEAN VELOCITY
ALLEN (1963)
FROM BALLADE (1953)
LOIRE RIVER
SAND WAVES
C = 15.1 V^2.41
V = SECTIONAL MEAN VELOCITY
DEPTH - 4.5 m
HEIGHT - 3.3 m
LENGTH - 128 m
SAINJON
(1871)
LOIRE RIVER
SAND BANKS
C = 11.2 (V^2 – 0.11)
V = SURFACE VELOCITY
SALSMAN ET AL. (1966)
ST. ANDREW BAY, FLORIDA
SAND RIDGE
C = 31.2 V^5
V = TEMPORAL MEAN FLOOD VEL. 55 cm ABOVE BED
DEPTH - 11 m
HEIGHT - 0.53 m
LENGTH - 18 m
MIGRATION RATE, C, M/DAY
0
1
2
3
4
0
0.1
0.2
0.3
0.4
0.5
0.6
0.7
FLUID FLOW VELOCITY, M/SEC, V

Figure 2. - Chesapeake Bay, the tidal entrance, and the study area of shoals and tidal channels.

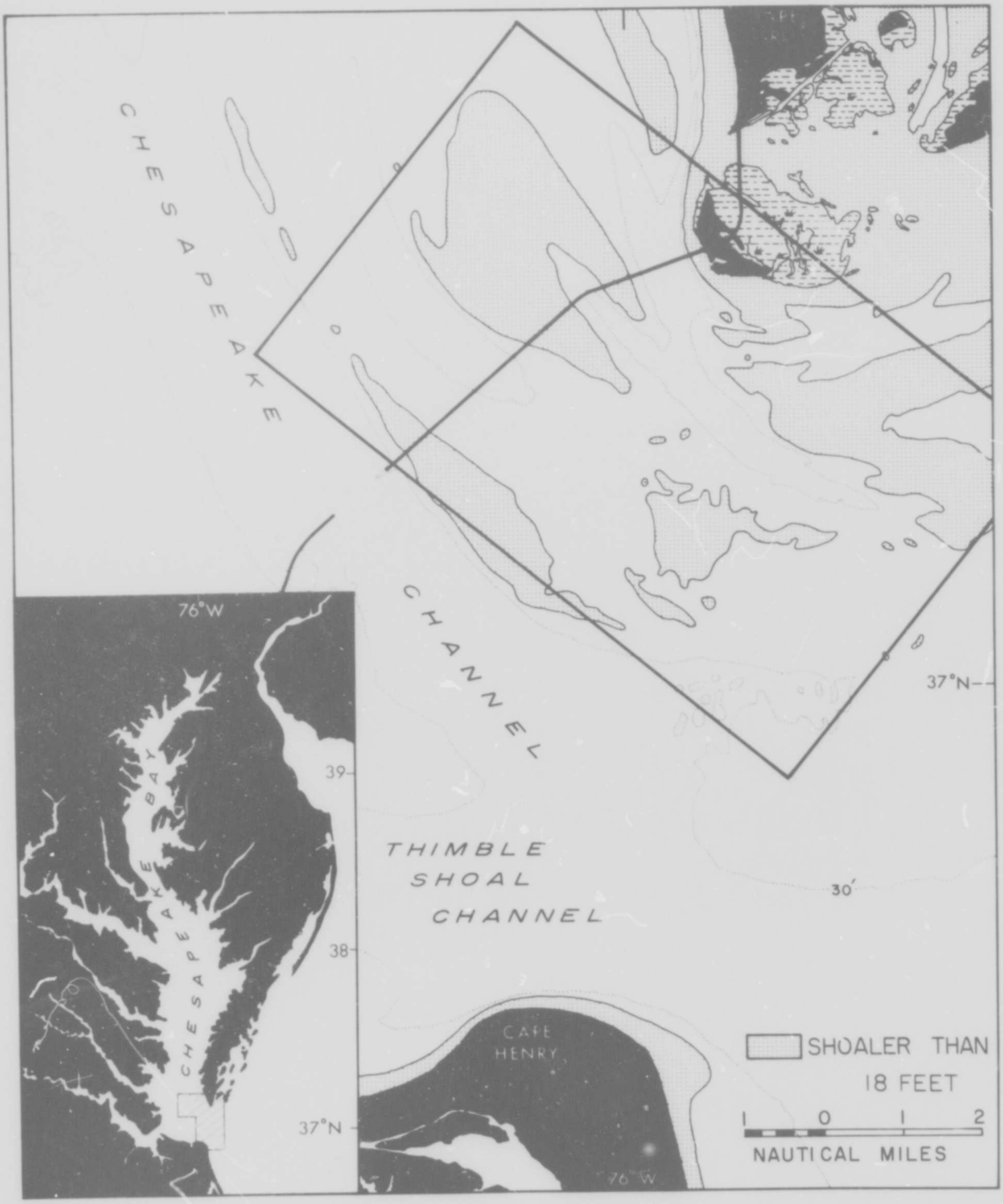
CHESAPEAKE
CHANNEL
THIMBLE
SHOAL
CHANNEL
CAPE
HENRY
37°N
30'
76°W
SHOALER THAN
18 FEET
1 0 1 2
NAUTICAL MILES
76°W
39
CHESAPEAKE BAY
38
37°N

Figure 3. - The sand bank and tidal channel area of Chesapeake Bay entrance. See Figure 2 for location.

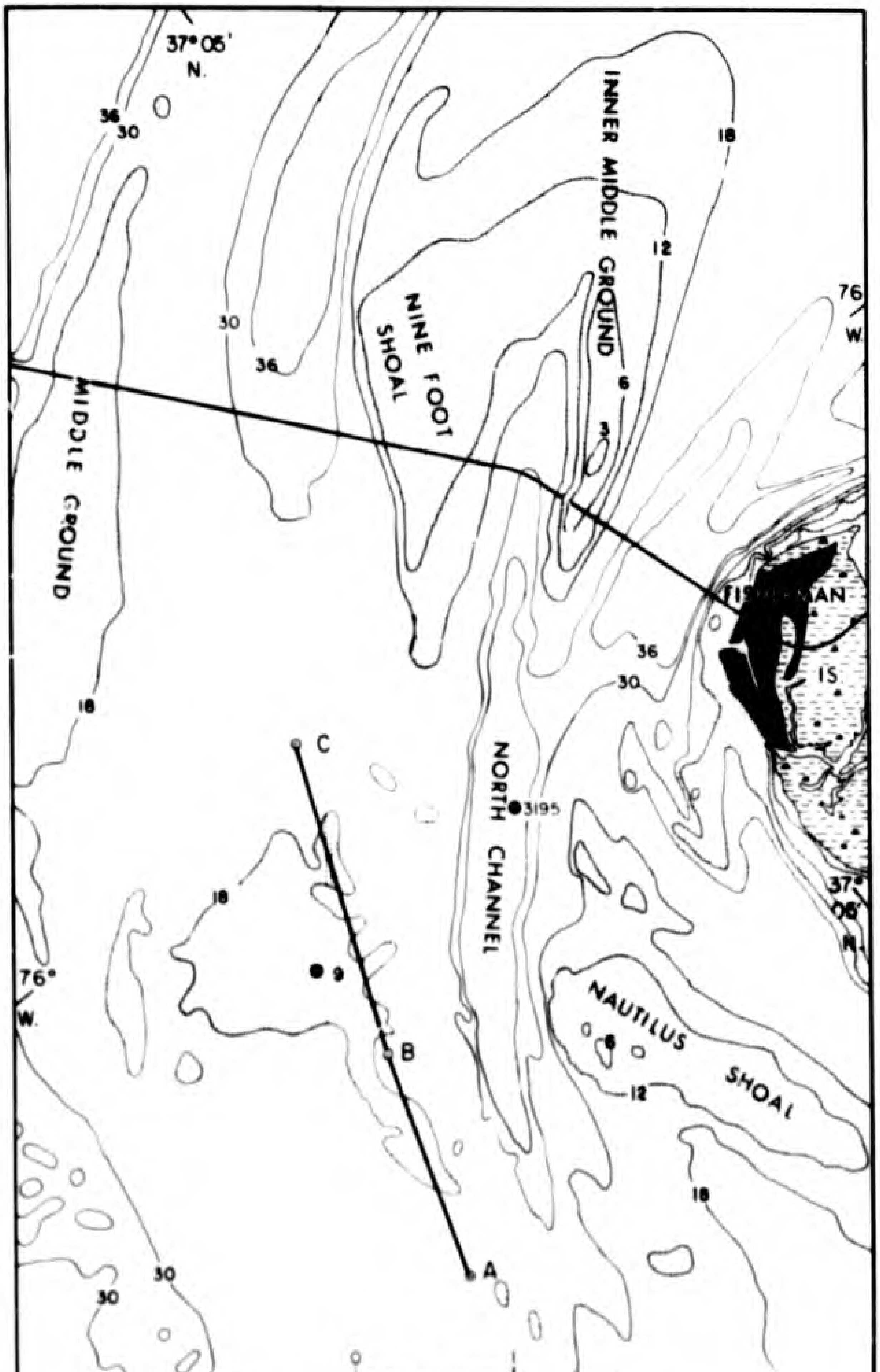
37° 05' N.
INNER MIDDLE GROUND
NINE FOOT SHOAL
MIDDLE GROUND
NORTH CHANNEL
NAUTILUS SHOAL
FISHERMAN IS.
76° W.
37° 05' N.
76° W.
3195
9
A
B
C
36
30
18
12
6
3
NAUTICAL MILES

Figure 4. - Tidal current speeds in North Channel (Station 3195, October 16-19, 1963) and atop a sand bank (Station 9, September 15-22, 1952). See Figure 3 for locations. Total depth at Station 3195 is 56 ft; current data are for a point 18.5 ft above the bed. Total depth at Station 9 is 16 ft; current data are for a point 5 ft above the bed. Estimated bed shear stress, τ_c, is given. Observed speeds were corrected to mean tidal range and averaged over 6-12 tidal cycles. Md is median diameter of the bed sediment, z_0 is the roughness length estimated from vertical velocity profile, k_s is the height of bottom roughness elements deduced from z_0, and is the critical shear stress, calculated from Shield's entrainment diagram.

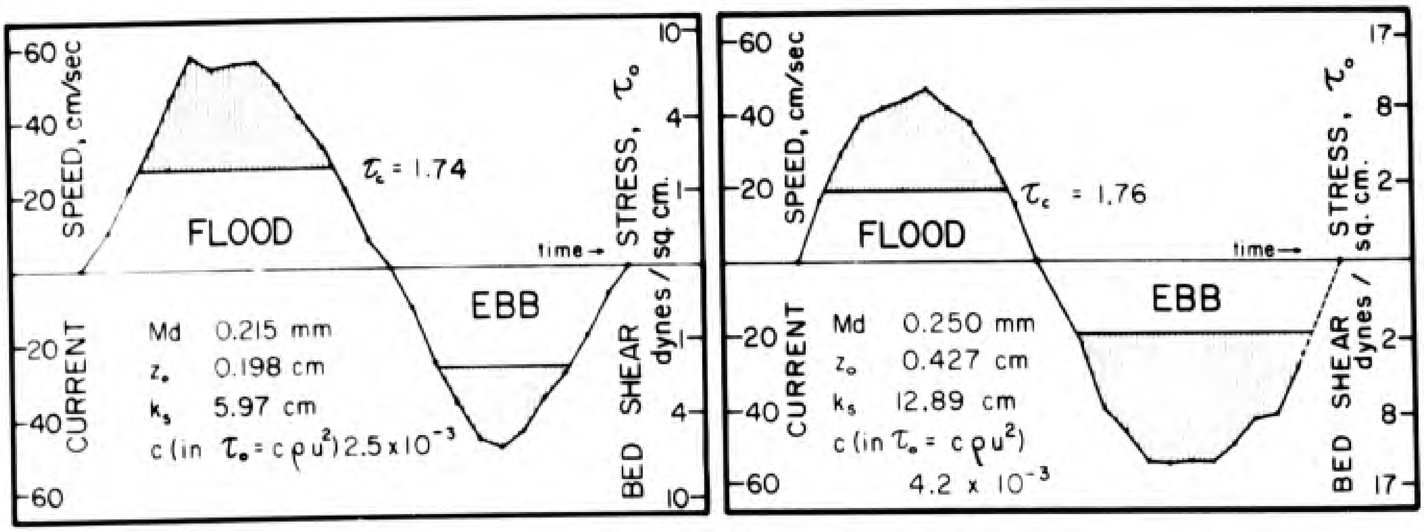

SPEED, cm/sec
CURRENT
FLOOD
EBB
τ_c = 1.74
time →
BED SHEAR STRESS, τ_o dynes / sq. cm.
Md 0.215 mm
z_o 0.198 cm
k_s 5.97 cm
c (in $\tau_o = c\rho u^2$) 2.5×10^{-3}
SPEED, cm/sec
CURRENT
FLOOD
EBB
τ_c = 1.76
time →
BED SHEAR STRESS, τ_o dynes / sq. cm.
Md 0.250 mm
z_o 0.427 cm
k_s 12.89 cm
c (in $\tau_o = c\rho u^2$)
4.2×10^{-3}

Figure 5. - Sand waves on profile A-B-C on December 29, 1969. Numbers designate sand wave crests and troughs for reference. The second profile is obtained by smoothing the first. The third profile is obtained by subtracting the second from the first. The lower diagrams are spectral density analyses of the indicated sections.

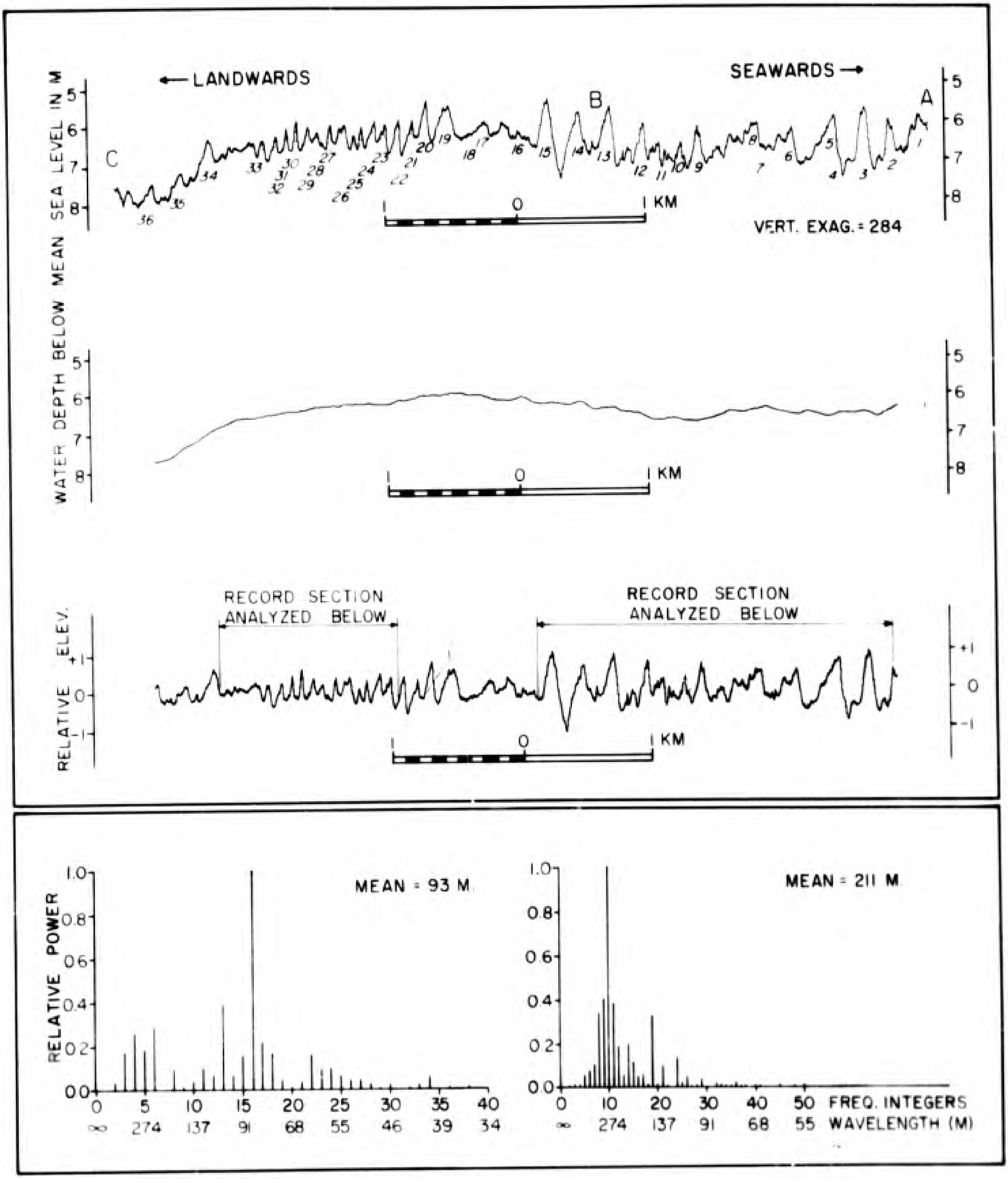

LANDWARDS
SEAWARDS
C
B
A
WATER DEPTH BELOW MEAN SEA LEVEL IN M
VERT. EXAG. = 284
KM
RECORD SECTION ANALYZED BELOW
RECORD SECTION ANALYZED BELOW
RELATIVE ELEV.
RELATIVE POWER
MEAN = 93 M.
MEAN = 211 M.
FREQ. INTEGERS
WAVELENGTH (M)

Figure 6. - Depth recorder profiles from parts of survey line A-B-C (see Fig. 3). Numbers under sand waves correspond to those of Figure 4. Vertical exaggeration is approximately 47X. Seaward is to the right, landward is to the left on each record. A1, asymmetrical-trochoidal highly peaked profiles of short wave length sand waves, September 12, 1969. A2, same features on November 8, 1969, showing low rounded form. A3, asymmetrical profiles of long wave length, with 6° foreslopes, September 9, 1970. A4, same, showing low rounded form on November 8, 1969. B1, step and hole on May 12, 1970. B2, same on June 27, 1969. B3, step and hole on November 25, 1969. C1, step on two sides of sand waves, on July 31, 1969. C2, same on August 28, 1969. C3, step on two sides of sand waves, on July 31, 1969. C4, same on August 28, 1969. D1, catbacks, on September 9, 1970. E1, complex trough topography on June 5, 1969. E2, same on June 5, 1969, second run of line. F1, small scale sand waves and other minor features, on June 27, 1969.

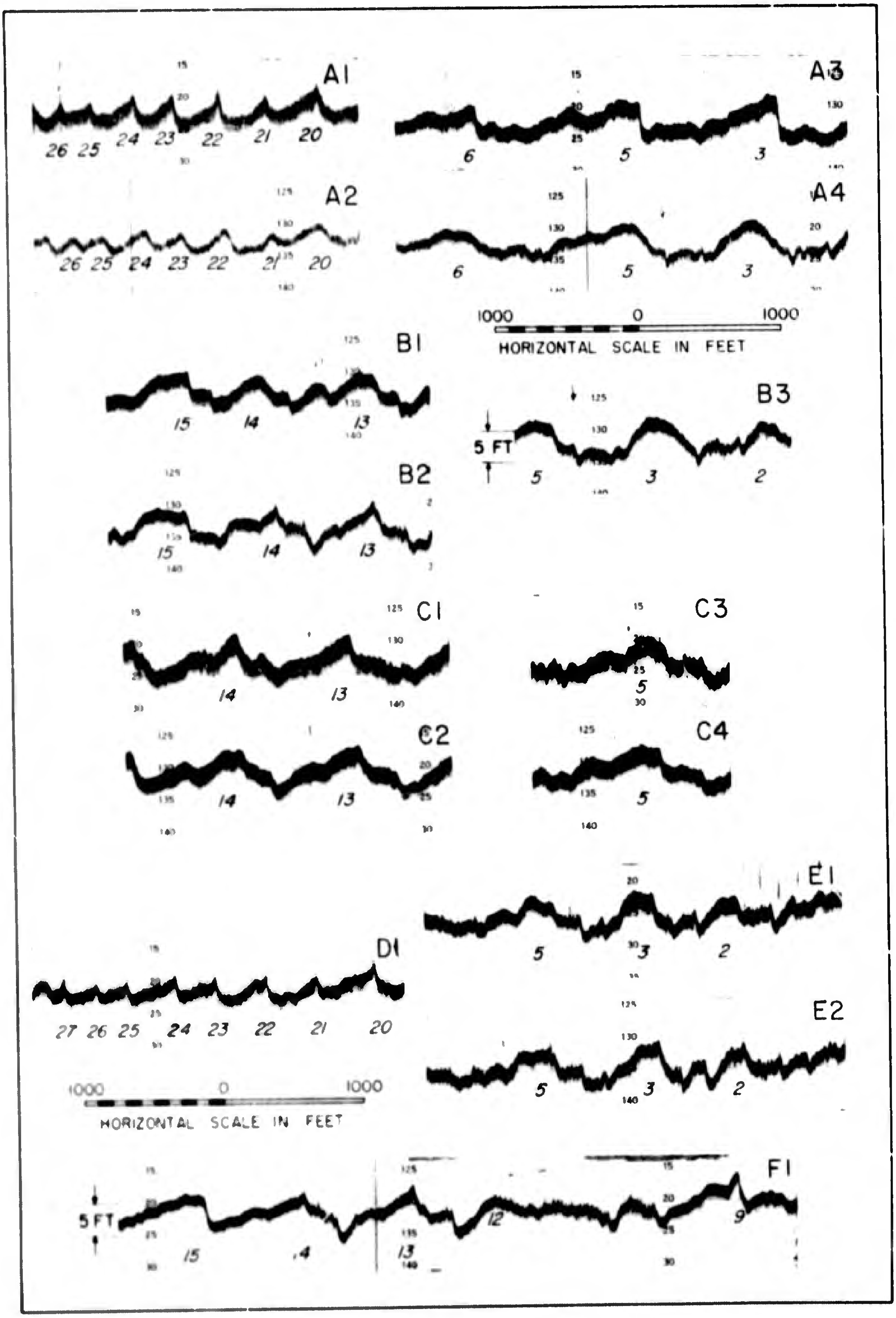
A1
26 25 24 23 22 21 20
A2
26 25 24 23 22 21 20
A3
6 5 3
A4
6 5 3
1000 0 1000
HORIZONTAL SCALE IN FEET
B1
15 14 13
B2
15 14 13
B3
5 FT
5 3 2
C1
14 13
C2
14 13
C3
5
C4
5
E1
5 3 2
E2
5 3 2
D1
27 26 25 24 23 22 21 20
1000 0 1000
HORIZONTAL SCALE IN FEET
F1
5 FT
15 14 13 12 9

Figure 7. - The dynamic environment of Chesapeake Bay entrance during the survey period. Heavy horizontal lines mark survey dates on which sand waves on profile A-B-C were notably high in relief and sharply peaked. Triangles denote these lines; the lowest number indicating the most characteristic record of this class. Dashed horizontal lines mark survey dates on which sand waves were notably low in relief and rounded. Half circles denote these lines; the lowest number indicating the most characterestic record of this class. Light horizontal lines mark survey dates on which sand waves were neither notably high nor notably low in relief.

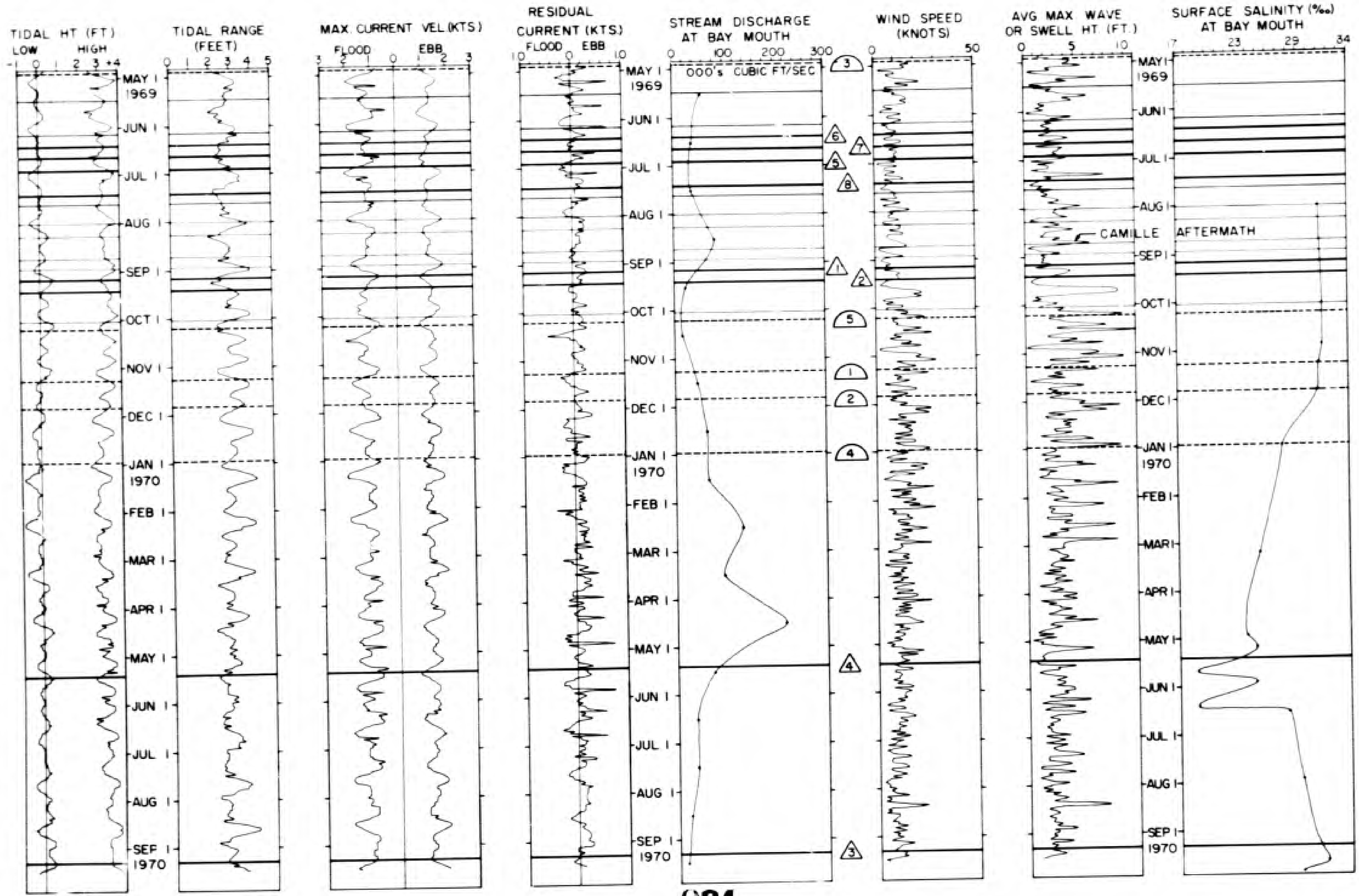
TIDAL HT (FT)
LOW HIGH
TIDAL RANGE (FEET)
MAX. CURRENT VEL.(KTS)
FLOOD EBB
RESIDUAL CURRENT (KTS.)
FLOOD EBB
STREAM DISCHARGE AT BAY MOUTH
000's CUBIC FT/SEC
WIND SPEED (KNOTS)
AVG MAX WAVE OR SWELL HT. (FT.)
SURFACE SALINITY (‰) AT BAY MOUTH
CAMILLE
AFTERMATH
MAY 1 1969
JUN 1
JUL 1
AUG 1
SEP 1
OCT 1
NOV 1
DEC 1
JAN 1 1970
FEB 1
MAR 1
APR 1
MAY 1
JUN 1
JUL 1
AUG 1
SEP 1 1970

Figure 8. - Typical travel-time curves for sand waves on the outer end of profile line A-B-C.

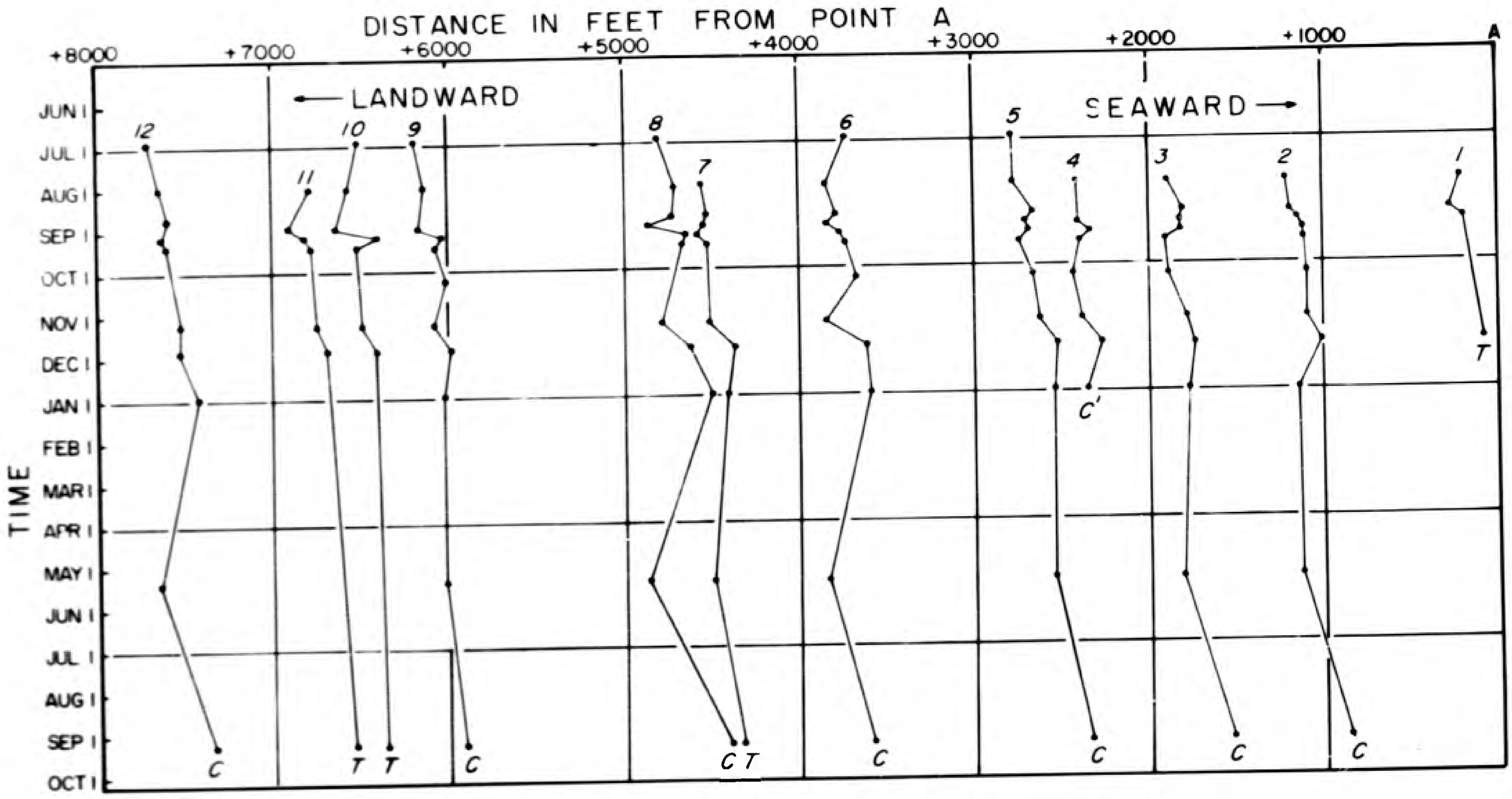

DISTANCE IN FEET FROM POINT A
+8000
+7000
+6000
+5000
+4000
+3000
+2000
+1000
A
← LANDWARD
SEAWARD →
TIME
JUN 1
JUL 1
AUG 1
SEP 1
OCT 1
NOV 1
DEC 1
JAN 1
FEB 1
MAR 1
APR 1
MAY 1
JUN 1
JUL 1
AUG 1
SEP 1
OCT 1
1
2
3
4
5
6
7
8
9
10
11
12
C
T
C'

Figure 9. - Upslope and downslope estimated ripple migration rates for ebb and flood flows over an idealized sand wave.

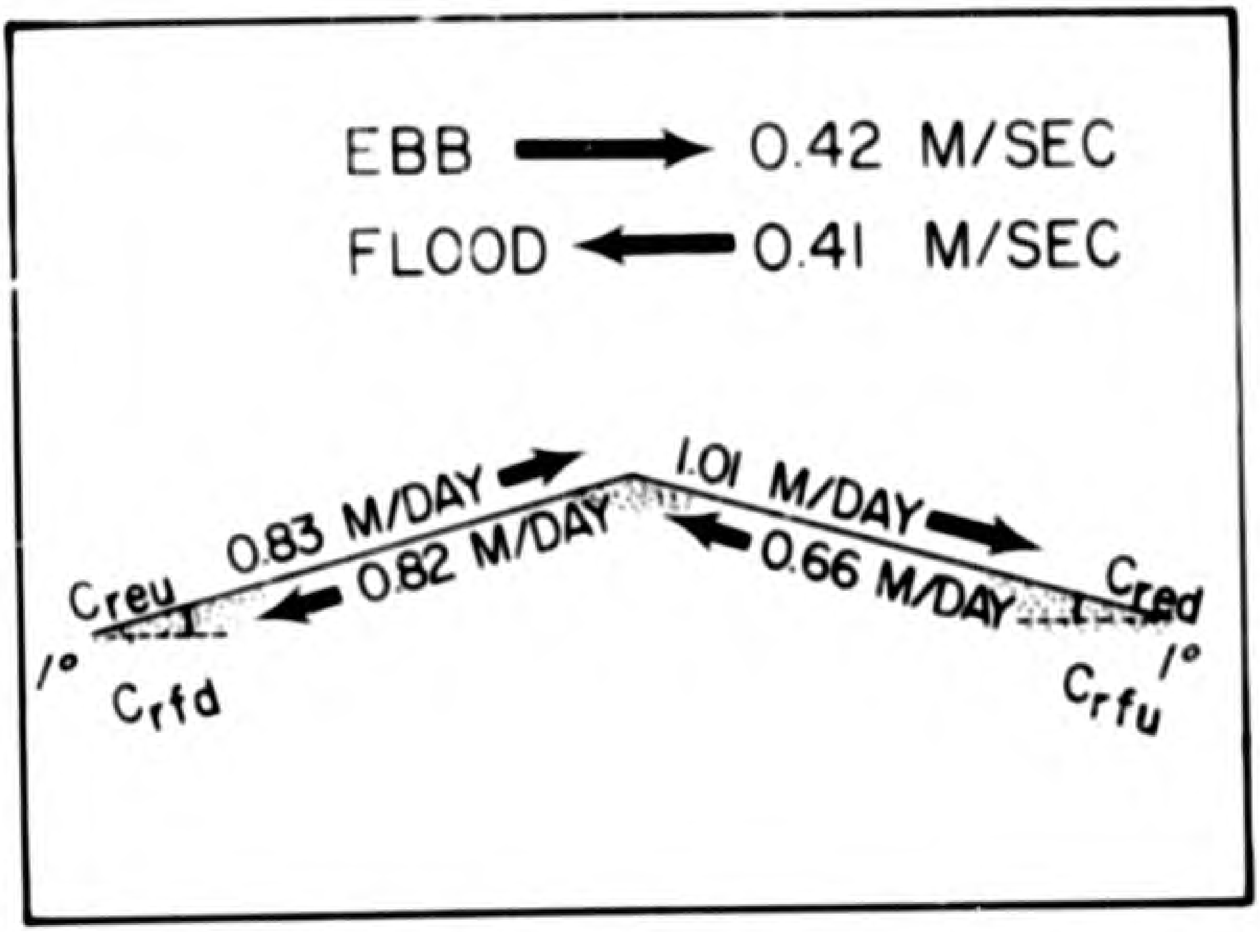
EBB 0.42 M/SEC
FLOOD 0.41 M/SEC
0.83 M/DAY
0.82 M/DAY
1.01 M/DAY
0.66 M/DAY
C_{reu}
C_{rfd}
C_{red}
C_{rfu}
1°
1°

Figure 10. - The ebb-flood tidal hydraulic environment of profile A-B-C.

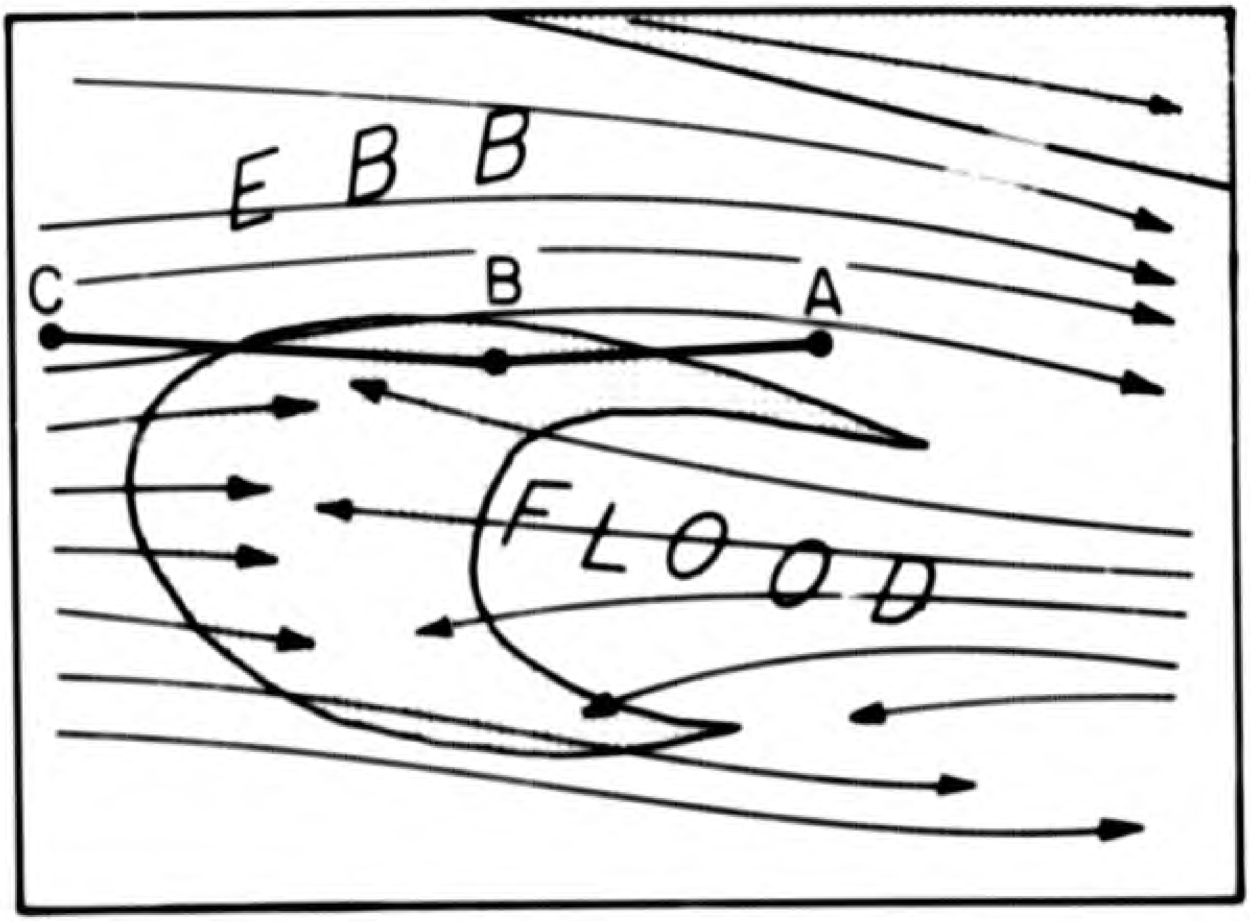
EBB
C
B
A
FLOOD

TABLE I

Migration Rates of Sand Waves on the Seaward Segment of Transect A-B-C in the Entrance Area to Chesapeake Bay, Virginia

Sand Wave Designation	Regression Coefficient (m/yr)	Significance P=	95% Confidence Limits (m/yr)	Position on Nov. 25, 1969 (m)
1 T	-150	<0.20	-102-402	A+21
2 C	- 61	<0.01	- 19-118	A+305
3 C	- 72	<0.01	- 31-112	A+530
4 C'	- 63	<0.20	- 37-163	A+690
5 C	- 89	<0.001	- 48-130	A+770
6 C	- 37	<0.20	- 18-93	A+1100
7 T	- 52	<0.02	- 14-90	A+1332
8 C	- 60	<0.02	- 19-140	A+1408
9 C	- 54	<0.01	- 24-85	A+1826
10 T	- 49	<0.10	- 10-108	A+1951
11 T	- 82	<0.01	- 37-127	A+2036
12 C	- 62	<0.05	- 11-113	A+2291
13 C	- 43	<0.20	- 12-99	A+2539
14 C	- 35	<0.40 NS	-	B+134
15 C	- 44	<0.20	- 11-99	B+378
16 T	- 53	<0.50 NS	-	B+570

T = prominent low between sand waves; C = sand wave crest; C' = small crest between larger sand waves; NS = not significant. Note: negative regression coefficient indicates seaward migration; positive regression coefficient indicates landward migration.

TABLE II

Migration Rates of Sand Waves on the Landward Segment of Transect A-B-C in the Entrance Area to Chesapeake Bay, Virginia

Sand Wave Designation	Regression Coefficient (m/yr)	Significance P=	95% Confidence Limits (m/yr)	Position on Nov. 25, 1969 (m)
17 C	-13	<0.90 NS	-	B+838
18 C'	+15	<0.90 NS	-	B+960
19 C	-15	<0.90 NS	-	B+1090
20 C	-25	<0.40 NS	-	B+1260
21 C	-21	<0.40 NS	-	B+1372
22 C	-27	<0.40 NS	-	B+1471
23 C	-27	<0.40 NS	-	B+1570
24 C	-25	<0.20	-17-66	B+1655
25 C	-33	<0.20	-14-31	B+1750
26 C	-27	<0.40 NS	-	B+1814
27 C	-27	<0.40 NS	-	B+1996
28 C	-34	<0.20	-23-91	B+2094
29 C	-39	<0.20	-24-103	B+2173
30 C	-31	<0.40 NS	-	B+2262
31 C	-20	<0.40 NS	-	B+2332
32 C	-14	<0.90 NS	-	B+2402
33 C	+ 2	<0.90 NS	-	B+2504
34 C	-34	<0.40 NS	-	B+2944
35 C	-26	<0.50 NS	-	B+3188
36 C	-24	<0.40 NS	-	B+3377

C = sand wave crest; C' = small crest between larger sand waves; NS = not significant. Note: negative regression coefficient indicates seaward migration; positive regression coefficient indicates landward migration.

Appendix A

Discriminant Analysis of

Sediments in the Mouth of

Chesapeake Bay, Virginia

by

William C. Smith

BLANK PAGE

According to Griffiths, classification is one of the basic steps in ordering a given complex of events. Any classification scheme requires a number of criteria for assigning objects to classes. These criteria are generally attributes which the individual objects have in common. Ideally, the classes that are established by the manipulation of the criteria are mutually exclusive and exhaustive.

Obviously, the most basic form of classification is one which subdivides a population of individuals into two classes. The criteria used to establish the classes should be the ones which would most likely lead to mutually exclusive and exhaustive classes. Fisher (1936) proposed the discriminant function as a statistical method for subdividing a number of individuals into previously defined classes on the basis of a number of common variables considered simultaneously. If two sets of samples can be clearly assigned to different classes established on the basis of a priori knowledge, they can be used to establish criteria for the classification of additional samples as well as testing the validity of the original classification.

In setting up a discriminant function it is necessary to define, on the basis of a priori knowledge, two classes which are mutually exclusive and exhaustive and to select properties of the individuals to be classified which will allow the assignment of each individual into one of the two classes. Usually the classes chosen possess various degrees of overlap so they are not mutually exclusive. In this case the assignment of an unknown individual to a class based on the application of the discriminant function has an associated probability of misclassification.

Various refinements and modifications are possible in establishing a discriminant function. It is possible, for example, to test whether a function based on ten properties is as effective as one based on a lesser number of properties. It is possible to encompass more than two classes by the establishment of a multiple discriminant function. There are also examples of both simple and multiple non-linear discriminants.

Discriminant analysis is a powerful multi-variate procedure which may be used in the classification of objects. It may be applied simply as a procedure to find some means of subdividing a population into two or more classes. Or, more likely, it may be a primary step in an attempt to establish relationships among groups of individuals with the ultimate objective of interpreting the relationships between the discriminated classes and among the properties of the classes which permit the discrimination.

The discriminant function is commonly used as a classification tool in the sciences. There are literally hundreds of articles ranging over several disciplines (biology, anthropology, psychology, medicine, economics, geology) and a wide variety of subject matters, some of which are discussed below.

It is in the realm of biology that we find the first applications of the discriminant function. Perhaps the best known example is a pioneering work in 1936 by Sir Ronald A. Fisher entitled "The Use of Multiple Measurements in Taxonomic Problems." In this paper Fisher used measurements obtained from the flowers of fifty plants of each of two species of iris (*I. setosa* and *I. versicolor*) to develop a numerical function that best classifies and separates the two species. Another early work is that of M. M. Barnard in 1935. In this study she applied the discriminant function to distinguish between four series of Egyptian skulls.

There are many other papers of anthropological, biological, and medical concern which make use of the technique. A few of these are mentioned below. Mahalanobis, et al. used the technique in an investigation of the skull characteristics of five different tribes in India. Linear discriminant functions were applied to four dimensions of fossil milk canines of Australopithecine in a paper by Bronowski and Long (1952) in order to decide which of two stated alternatives is preferred; ape or human. Jolcoeur (1959) uses discriminant analysis based on twelve skull dimensions in discussing geographic variation in the wolf, Canis lupus.

One example of the use of discriminant functions in medical research is found in a report by Wirta and Taylor (1970) on the development of a myoelectrically controlled prosthetic arm for above-elbow amputees. In order to make the arm truly effective it was necessary to determine which synergistic muscle groups in the back, chest, and shoulders would allow the subject to perform eight desired types of movement with minimum cognitive effort. The use of discriminant functions proved to be ideal for this purpose.

Discriminant function analysis has recently come into its own in the geosciences. A few applications follow below: Mellon (1964) has used the method to establish parameters controlling the cement distribution of sandstone. Griffiths (1957) differentiated between uranium bearing and barren sediments. Middleton (1962) shows that the chemical composition of sandstone varies significantly with the tectonic environment of the basin of deposition. McIntyre (1961) used heavy minerals in a comparison of three different environmental settings (glacial till, fluvioglacial delta, and beach sands). It has been shown by Potter, et al. (1963) that marine and fresh water shales can be distinguished by applying discriminant analysis to trace element contents in a sample. Chayes (1965) uses a discriminant function to classify igneous rocks plotted in a ternary diagram in terms of 3 normative end members. He also used the technique to distinguish basaltic lavas of circum-oceanic and oceanic types. Sahu (1964) shows the sand from various environments (dune, beach, shallow water, etc.) can be distinguished using a discriminant function based on textural parameters. Miller (1954) shows that the environment can be discriminated by the textural properties of the sediments in each environment.

As previously mentioned, Fisher's discriminant function and the closely related generalized distance (D^2) of Mahalanobis were developed for discriminating between similar plant or animal species by means of multiple measurements. The discriminant function is essentially a weighted average of a set of measurements. The computed weights compensate for redundancy which tends to occur due to intercorrelations between measurements. D^2 is the sum of squares of differences between corresponding mean values of two sets of measurements and may be interpreted as the "distance" between the means of the two groups.

An appropriate problem for discrimination would be one in which the data may be divided on a priori grounds into two or more groups. The discriminant function may then be defined as the linear function which best separates the groups of measures. "Best" discrimination occurs when the ratio of the between means of groups sums of squares to the within groups sums of squares is maximized (Middleton, 1962).

The argument may also be expressed geometrically. Consider a multi-variate (K variables) sample as a point in a multi-dimensional (K) space. A cluster of these sample points in K dimensional space defines a population. A second population described by the same variables forms another cluster of points. It is now desired to compute a K dimensional plane that provides the best separation between the two clusters. Any unknown sample may be classified as belonging to a population depending on which side of the K plane it falls. The locations of the populations are described by the K dimensional coordinates of their multi-variate means. The distance between the multi-variate means is a measure of the degree of distinctness of the two populations.

The discriminant function may be developed mathematically as follows from Davis and Sampson (1966). A set of n_1 samples consisting of variables A_1, B_1, C_1 . . . K_1 is taken from population 1. A second set of samples (n_2) with the same K variables is taken from population 2. Then the sums of variables, sums of squares of the variables, and sums of cross products for each population sample are computed. They are then used in the following series of equations to produce the discriminant function.

(1) $\bar{A}_1 = \dfrac{\Sigma A_1}{n_1}$ $\qquad \bar{A}_2 = \dfrac{\Sigma A_2}{n_2}$

$\vdots \qquad\qquad \vdots$

$\bar{K}_1 = \dfrac{\Sigma K_1}{n_1}$ $\qquad \bar{K}_2 = \dfrac{\Sigma K_2}{n_2}$

(2) $\Delta\bar{A} = \bar{A}_1 - \bar{A}_2$

$\vdots$

$\Delta\bar{K} = \bar{K}_1 - \bar{K}_2$

(3) $$SS_A = (\Sigma A_1^2 + \Sigma A_2^2) - \left[\frac{(\Sigma A_1)^2}{n_1} + \frac{(\Sigma A_2)^2}{n_2}\right]$$

$\vdots$

$$SS_K = (\Sigma K_1^2 + \Sigma K_2^2) - \left[\frac{(\Sigma K_1)^2}{n_1} + \frac{(\Sigma K_2)^2}{n_2}\right]$$

(SS_A . . . SS_K are unbiased estimates of the pooled variances of the K variables)

(4) $$SS_{AB} = (\Sigma A_1B_1 + \Sigma A_2B_2) - \left[\frac{\Sigma A_1 \Sigma B_1}{n_1} + \frac{\Sigma A_2 \Sigma B_2}{n_2}\right]$$

$$SS_{AC} = (\Sigma A_1C_1 + \Sigma A_2C_2) - \left[\frac{\Sigma A_1\ \Sigma C_1}{n_1} + \frac{\Sigma A_2\ \Sigma C_2}{n_2}\right]$$

.

.

.

$SS_{AK} =$

.

$SS_{BC} =$

.

$SS_{BK} =$

.

$SS_{(K-1)K} =$

AB, AC, . . . (K-1)K represent all possible combinations of the K variables. The number of combinations is equal to $\binom{K}{2}$, or in the case of 4 variables $\left(\frac{4!}{2!2!}\right) = 6$. SS_{AB}, SS_{AC}, . . . $SS_{(K-1)K}$ are unbiased estimates of the covariance of the variable. Variance and covariance estimates are set into linear equations which are equated to the values $\Delta\bar{A}$, $\Delta\bar{B}$, ... , $\Delta\bar{K}$ times the constant $(n_1 + n_2 - 2)$

$$(5) \qquad SS_A\lambda_a + SS_{AB}\lambda_b + SS_{AC}\lambda_c + \ldots\ldots + SS_{AK}\lambda_k = \Delta\bar{A}(n_1 + n_2 - 2)$$

.

.

$$SS_{AB}\lambda_a + SS_B\lambda_b = SS_{AC}\lambda_c = \ldots\ldots + SS_{AK}\lambda_k = \Delta\bar{B}(n_1 + n_2 - 2)$$

.

.

$$SS_{AK}\lambda_a + SS_{BK}\lambda_b + SS_{CK}\lambda_c + \ldots\ldots\ldots + SS_K\lambda_k = \Delta\bar{K}(n_1 + n_2 - 2)$$

The K simultaneous equations are then solved to produce values of λ_a, λ_b, λ_c, ... λ_k. The discriminant function $\bar{a}$ is in the form

$$(6) \qquad \bar{a} = \lambda_a A + \lambda_b B + \lambda_c C + \ldots\ldots + \lambda_k K$$

$\bar{a}_o$, the discriminant index may be found by using the means of the combined population samples in the discriminant function.

$$(7) \qquad \bar{a}_o = \lambda_a \frac{\Sigma A_1 + \Sigma A_2}{n_1 + n_2} + \lambda_b \frac{\Sigma B_1 + \Sigma B_2}{n_1 + n_2} + \lambda_k \frac{\Sigma K_1 + \Sigma K_2}{n_1 + n_2}$$

Discriminant values for each population sample are found by substituting the means for each set of data into equation (6). An unknown sample may be assigned to either of the two populations by substituting the appropriate value of the variables into the discriminate function. If the value obtained is on the $\bar{a}_1$ side of $\bar{a}_o$ the sample is assigned to population 1. If on the $\bar{a}_2$ side of $\bar{a}_o$ it is assigned to population 2. Since $\bar{a}_o$ is the computed plane which bisects the space between sample clusters the probability of misclassifying a sample from either population 1 or 2 is equal.

Since discriminant analysis is based on the assumption that two samples are drawn from different populations it is desirable to test the statistical distinctness of the multi-variate means of the two groups. A significance test may be derived from the generalized distance (D^2) of Mahalanobis. D^2 is derived by Middleton (1962) by substituting the differences between the variable means into the discriminant function as follows:

$$(8) \qquad D^2 = \lambda_a \Delta \bar{A} + \lambda_b \Delta \bar{B} + \lambda_c \Delta \bar{C} + \, . \, . \, . \, . \, . + \lambda_k \Delta \bar{K}$$

A test of significance for the multi-variate means is given by:

$$(9) \qquad F_{K,\, n_1 + n_2 - K - 1} = \left[\frac{n_1 n_2}{(n_1+n_2)\ (n_1+n_2-2)} \right] \left[\frac{n_1+n_2-K-1}{K} \right] \times D^2$$

The contribution by each variable to the total distance between multi-variate means is given by

$$(10) \qquad \% \text{ contributed by } A = (\lambda_a \Delta \bar{A} / D^2) \times 100$$

$$\% \text{ contributed by } B = (\lambda_b \Delta \bar{B} / D^2) \times 100$$

Variables making insignificant contributions to D^2 can be detected in this manner. One slight drawback is that the equation tests only for the contribution of the variable under consideration and does not consider contribution made between variables that are highly correlated. If the variables are not truly independent, their interactions contribute more strongly to D^2 than the test shows. Since one of the assumptions of the discriminate function is an independence of variables, known dependent variables should not enter into the computations.

Equation 10 permits the elimination of variables with low contributions to D^2. These can be eliminated on successive runs until the F test (equation 9) for significance of difference between the multi-variate means is reduced below the value of the assigned significance level. Even though all variables contribute to the function, it is desirable to limit consideration to those that give the desired degree of discrimination.

The program used to compute the discriminant function for two sample groups is one modified for use by an I.B.M. 1130 computer. The original program by Davis and Sampson was for use by an I.B.M. 1620 computer. The program can use up to 20 variables and have any number of samples in either sample group. Sums, sums of squares, and sums of cross-products are accumulated as the data are read into the computer. Unbiased estimates of sample variances and covariances (equations 3 and 4) are computed and become terms in K simultaneous equations. These equations are then solved for λ_k by a modification of the Gauss - Jordan method. The λ_k terms are constants in the linear discriminant function.

Program output consists of constant terms (λ_k), the discriminant index ($\bar{R}_0$), the discriminant values ($\bar{R}_1$ and $\bar{R}_2$), for each of the two groups, Mahalanobis' Generalized Distance (D^2), and the percent contributed by each variable to D^2. An F value for determining significance is also obtained.

It has been noted that there are two distinctive sand types found in the mouth of the Chesapeake Bay. The first, hereafter called the "brown" population is definitely brownish in color, relatively coarse grained, and has a low percentage by weight of material finer than 0.062 mm. The second or "gray" population is definitely grayish in color, relatively fine grained, and has a relatively high percentage by weight of material finer than 0.062 mm.

There were 95 samples that were easily classified by visual inspection. These samples (40 brown and 55 gray) serve to establish a priori classes into which all subsequent samples can be catalogued by discriminant function analysis.

Four variables were chosen to build a series of discriminant functions. These variables and the Z scores for all samples are listed in Table I. The variables are as follows:

Variable (1). Intermediate diameter of the coarsest grain, (largest quartz or worn crystalline rock fragment in the sample).

Variable (2). Intermediate diameter of the coarsest hydraulically active shell.

Variable (3). Weight percentage of material finer than 0.062 mm.

Variable (4). Water depth.

Eleven discriminant functions were built using all combinations of the four variables. Two "discriminated" better than the others. These were the function constructed using all four variables and that using the coarsest grain and weight percentage of material finer than 0.062 mm. Even though the function using the four values is the more significant (see Table II) the one using the coarsest grain and weight percentage "fines" was chosen as the classifatory tool. This decision may be justified by several reasons: (1) The contribution to D^2 by the coarsest grain (96.94%) and weight percentage "fines" (14.03%) is much higher than that contributed by the coarsest shell (-11.68%) and water depth (0.70%). (2) Coarsest grain and weight percentage "fines" are direct measurements of the sample itself as opposed to water depth and are always easily and accurately obtained while water depth may not be. (3) There is good correlation between the coarsest grain and coarsest shell measurements (Ludwick, 1970, Appendix B, Figure 6). As the discriminant function is bases on the assumption of independence of variables known sets of dependent variables should not be included. Therefore, since the coarsest shell measurement makes a negligible contribution to D^2, it may be eliminated.

An interesting comparison may be made between Figure 3 and Figure 4. Figure 3 shows the geographical distribution of the "brown" and "gray" sands as determined by discriminant function analysis. Figure 4 (Ludwick, 1970, Appendix B, Figure 3) shows the geographic distribution of the maximum grain. The very close (indeed, almost identical) distribution of "brown" sands and those samples with a maximum intermediate diameter greater than 2.5 mm. should be noted. The same applies for the "gray" sands and those samples with an intermediate diameter less than 2.5 mm. This is another indication of the effectiveness of the coarsest grain measurement as a discriminating agent.

The majority of the coarsest measurements and the "brown" sands are concentrated in one area. Coupled with other information (such as the shape of the shoals and the fact that the brown coloring may be due to iron-staining) this cluster of samples may mark the sand banks in the aforementioned area as relict features which are in equilibruim with a former hydraulic regime and are presently being modified by waves and currents.

Miller, R. L., 1954. A model for the analysis of environments of sedimentation. J. Geol., 72: 786-809.

Potter, P. E., Shimp, N. F. and Witters, J., 1963. Trace elements in marine and fresh water argillaceous sediments. Geochim. et Cosmochim. Acta, 27: 669-694.

Shau, B. K., 1964. Depositional mechanisms from the size analysis of clastic sediments. J. Sediment. Petrol., 34: 73-83.

Wirta, R. W. and Taylor D. R., 1970. Multiple axis myoelectrically controlled prosthetic arm, Final Report. U.S. Dept. of Health, Education and Welfare, RD-2169-M, 50 pp.

REFERENCES

Barnard, M. M., 1935. The secular variations of skull characters in four series of Egyption skulls. Annals of Eugenics, 6: 352-371.

Bronowski, J. and Long, W. M., 1952. Statistics of discrimination in anthropology. Am J. Phys. Anthrop.,10: 385-394.

Chayes, F., 1965. Classification in a ternary diagram by means of discriminant functions. Am. Mineralogist, 50: 1618-1633.

Chayes, F. and Velde, D., 1965. On distinguishing basaltic lavas of Circum-oceanic and Oceanic-Island type by means of discriminant functions. Am. J. Science, 263: 206-222.

Davis, J. C. and Sampson, R. J., 1966. Fortran II Program for Multivariate Discriminant Analysis Using an I.B.M. 1620 Computer. Computer Contribution 4, State Geological Survey, the University of Kansas, Lawrence, 1-8 pp.

Fisher, R. A., 1936. The use of multiple measurements in taxonomic problems. Annals of Eugenics, 7: 179-188.

Griffiths J. C., 1957. Petrographic investigation of the Salt Wash sediments, Final Report. U.S. Atomic Engery Comm. R.M.E.-3151, 38 pp.

Griffiths, J. C. 1966. Application of discriminant functions as a classification tool in the geosciences. In: D. F. Merrian (Editor), Computer Applications in the Earth Sciences: Colloquim on Classification Procedures. Computer Contribution 7, State Geological Survey, the University of Kansas . Lawrence, 48-52 pp.

Jolicoeur, P., 1959. Multivariate geographical variation in the wolf Canis lupus. Evolution, 13: 283-299.

Ludwick, J. C., 1970. Sand waves and tidal channels in the entrance to Chesapeake Bay, Technical Report. Geography Branch, Office of Naval Research, N00014-70C-0083, 107 pp.

Mahalonobis, P. C., Majumdar, D. N. and Rao, C. R., 1949. Anthropometric survey of the United Provinces 1941, a statistical study. Sankhya, 9: 90 pp.

McIntyre, D. D., 1961. A comparison of three association environments, glacial till, fluvioglacial delta and beach sand, in terms of their quartz, garnet, and hornblende grains, Min. Ind. Expt. Sta. Pub., the Pennsylvania State University, 78 pp.

Mellon. G. B., 1964. Discriminatory analysis of calcite-and silicate-cemented phases of the Mountain Park Sandstone. J. Geol., 72: 786-809.

Middleton, G. V., 1962. A multivariate statistical technique applied to the study of sandstone composition. Trans. Royal Soc. Canada, 56 Ser. III, Sec. III: 199-126.

Figure 1. - Sample location map. The numbers below are sample numbers keyed to the diagram.

Line 1A-1B	Line 2A-2B	Line 3A-3B	Line 4A-4B	Line 5A-5B	Line 6A-6B	Line 7A-7B	Line 8A-8B	Line 9A-9B	Line 10A-10B
1-1	12-199	12-200	12-201	3-24	8-156	5-92	2-9	6-110	9-167
1-3	12-198	4-71	10-168	3-25	8-155	5-91	2-10	6-109	9-166
1-5	7-131	4-70	10-169	3-26	8-154	5-90	2-11	11-194	9-165
1-6	7-130	4-69	10-170	3-27	8-153	5-89	11-195	2-13	9-164
	7-129	4-68	10-171	3-28	8-152	5-88	11-197	6-107**	9-163
	7-128	4-67	10-172	3-29	8-151	5-87	11-196	6-106	9-162
	7-127	4-66	10-173	3-30	8-150	5-86	2-12	6-105	9-161
	7-126	4-65	10-174	3-31	8-149	5-85	6-107*	6-104	9-160
	7-125	4-64	10-175	3-32	8-148	5-84	2-13	6-103	9-159
	7-124	4-63	10-176	3-33	8-147	5-83	2-14	6-102	9-158
	7-123	4-62	10-177	3-34	8-146	5-82	2-15	6-101	9-157
	7-122	4-61	10-178	3-35	8-145	5-81	2-16	6-100	
	7-121	4-60	10-179	3-36	8-144	5-79	2-19	6-99	
	7-120	4-59	10-180	3-37	8-143	5-78	2-17	6-98	
	7-119	4-58	10-181	3-38	8-142	5-77	2-18	6-97	
	7-118	4-57	10-182	3-39	8-141	5-76	2-20	6-96	
	7-117	4-56	10-183	3-40	8-140	5-75	2-21	6-94	
	7-116	4-55	10-184	3-41	8-139	5-74	2-22	6-93	
	7-115	4-54	10-185	3-42	8-138	5-73	2-23		
	7-114	4-53	10-186	3-43	8-137	5-72			
	7-113	4-52	10-187	3-44	8-136				
	7-112	4-51	10-188	3-45	8-135				
	7-111	4-50	10-189	3-46	8-134				
		4-49	10-190		8-133				
		4-48	10-191		8-132				
		4-47	10-192						
			10-193						

*Intersects line 9A-9B at this point.

**Intersects line 8A-8B at this point.

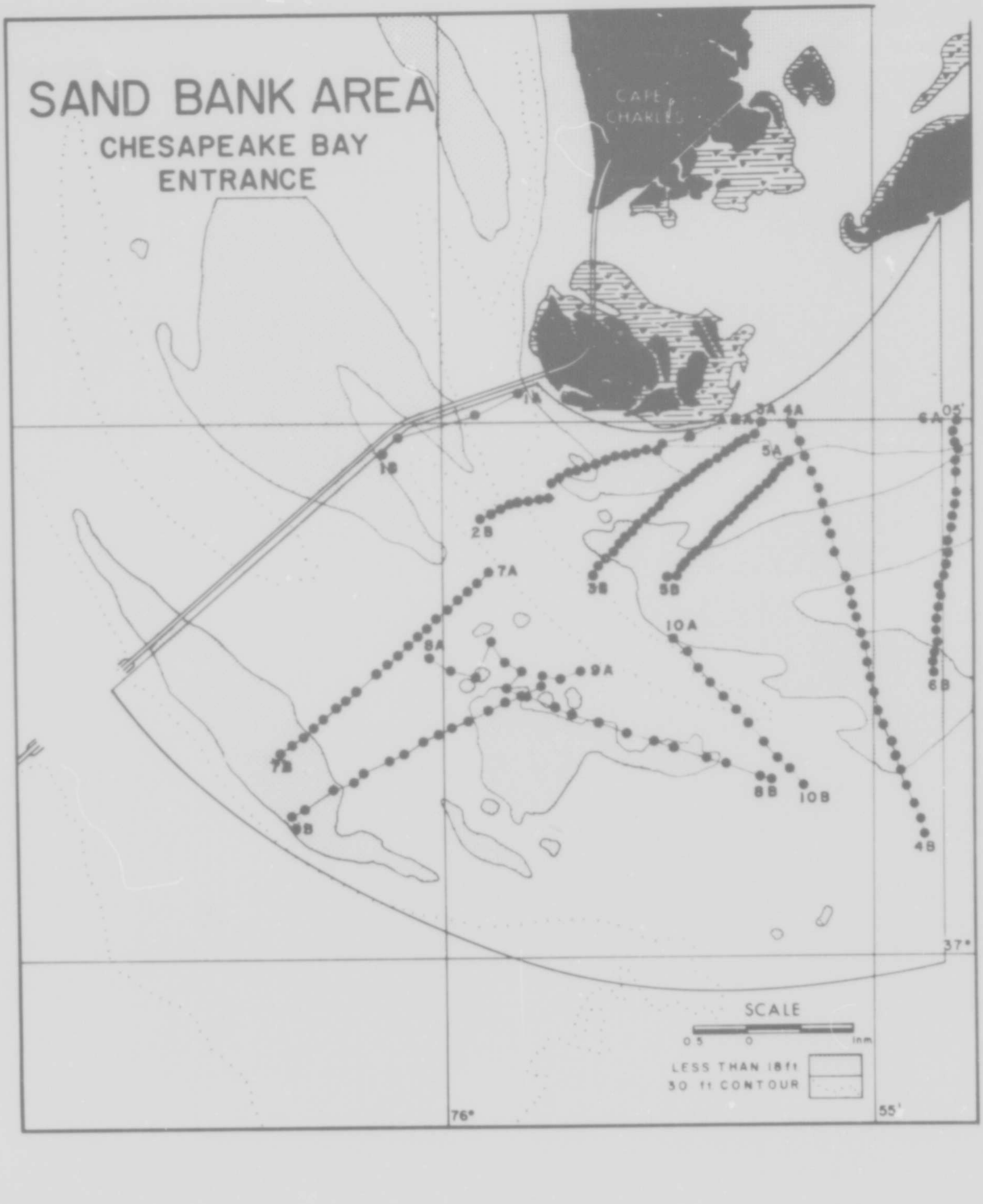
SAND BANK AREA
CHESAPEAKE BAY
ENTRANCE
CAPE CHARLES
1A
1B
2B
3A
4A
5A
6A
05'
3B
5B
7A
10A
8A
9A
6B
7B
8B
10B
9B
4B
37°
SCALE
LESS THAN 18 ft
30 ft CONTOUR
76°
55'

Figure 2. - This histogram is based on the $\mathcal{Z}$ scores of the samples (55 "gray", 40 "brown") that were selected by visual inspection to form the two *a priori* classes on which the discriminant function is based. This is a two-fold function, the variables being intermediate diameter of the coarsest grain and weight percentage of material finer than 0.062 mm. Reasons for choosing these variables are discussed in the text.

All samples whose $\mathcal{Z}$ scores fall to the right of $\mathcal{Z}_0$ (the discriminant index) are classified as brown sands all falling to the left are classified as gray sands. $\mathcal{Z}_g$ is the mean $\mathcal{Z}$ score of the gray population, $\mathcal{Z}_B$ that of the brown population. The generalized distance, Mahalanobis D^2, between the two population means is 3.9688. Coarsest grain contributes more to the discrimination than weight percentage "fines" (84.8079% vs. 15.1920%). The F value for 2 and 92 degrees of freedom is 45.4608 making the discriminant function significant at the 95 percent level.

Fourteen (9 brown and 5 gray) of the 95 samples used to delineate the two populations were misclassified. Those that were visually selected as brown but which discriminant analysis classifies as gray are denoted by "B" in the gray area of the histogram. Those visually selected as gray but are classified by discriminant analysis as brown are denoted by "G" in the brown area of the histogram. Four samples are not represented. These are the three "brownest" samples with $\mathcal{Z}$ scores of 10.5071, 10.3621, and 9.0354 and the "grayest" sample with a $\mathcal{Z}$ score of -3.9760.

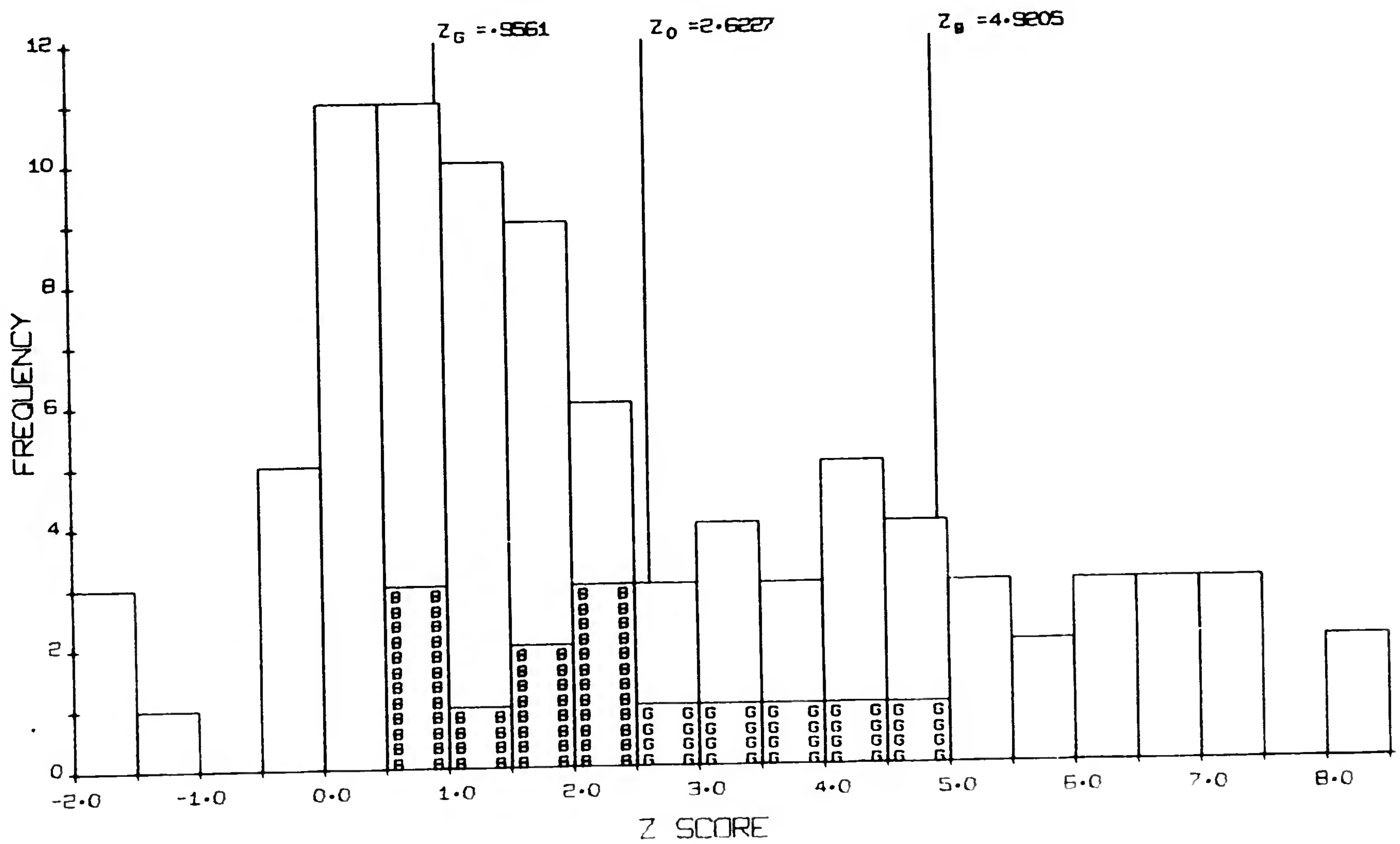

Z_G =·9561
Z_O =2·6227
Z_B =4·9205
FREQUENCY
0
2
4
6
8
10
12
-2·0
-1·0
0·0
1·0
2·0
3·0
4·0
5·0
6·0
7·0
8·0
Z SCORE

Figure 3. - This figure shows the geographical distribution of the "brown" and "gray" sands as determined by discriminant function analysis. The two extreme "brown" samples ($Z = 10.5071$ and $Z = 10.3621$) and the two extreme "gray" samples ($Z = -3.9760$ and $Z = -1.7438$) are denoted by asterisks.

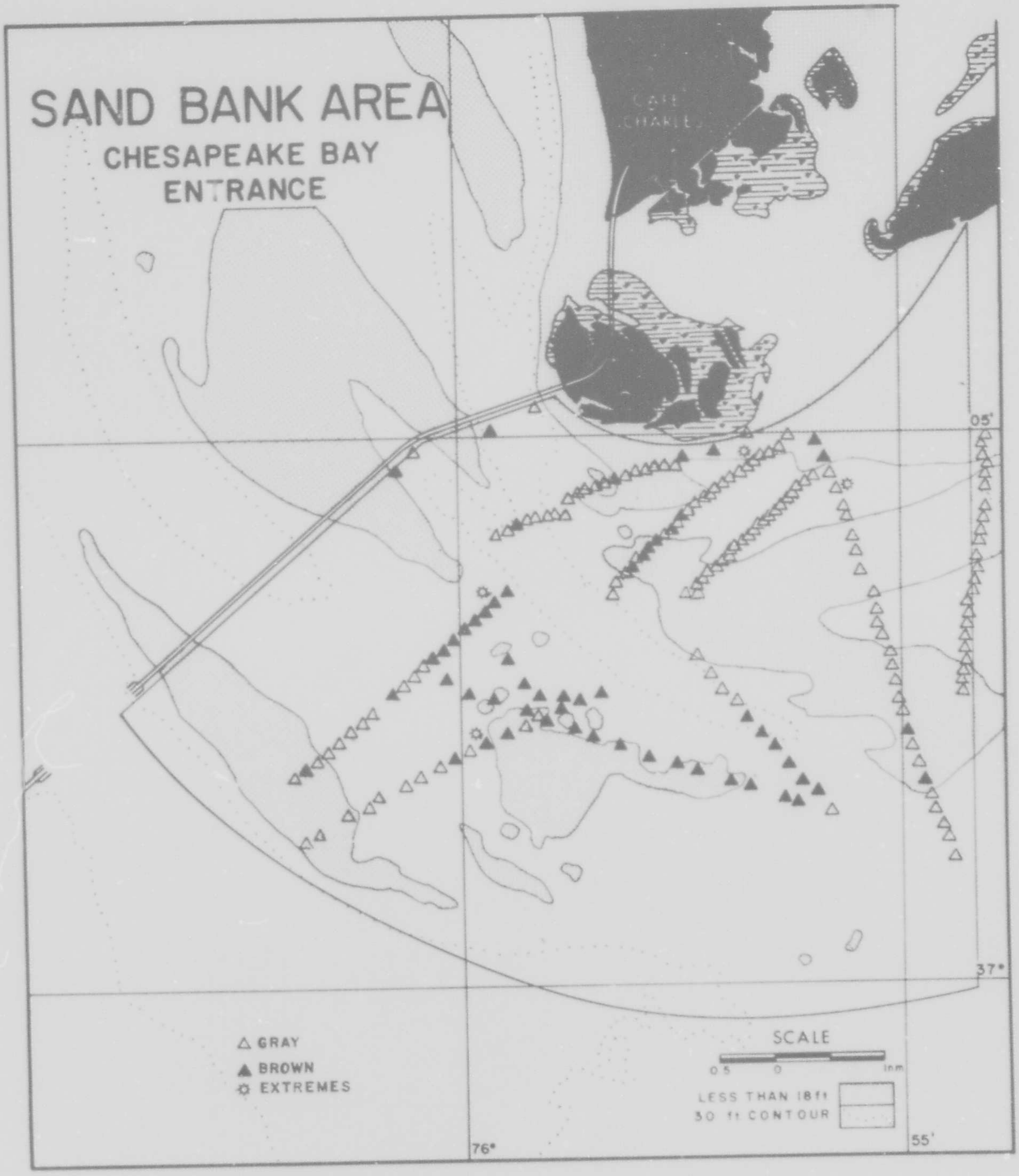
SAND BANK AREA
CHESAPEAKE BAY
ENTRANCE
CAPE CHARLES
05'
37°
76°
55'
△ GRAY
▲ BROWN
☼ EXTREMES
SCALE
0.5
0
1nm
LESS THAN 18ft
30 ft CONTOUR

Figure 4. - This figure shows the geographical distribution of maximum grain (i.e. intermediate diameter of the coarsest grain of quartz or worn crystalline rock fragment). Shown are two classes, the boundary between which was determined by trial and error so as to maximize the geographic coherence of the pattern. The two extreme coarsest grain, 8.12 mm. and 8.59 mm., are denoted by asterisks.

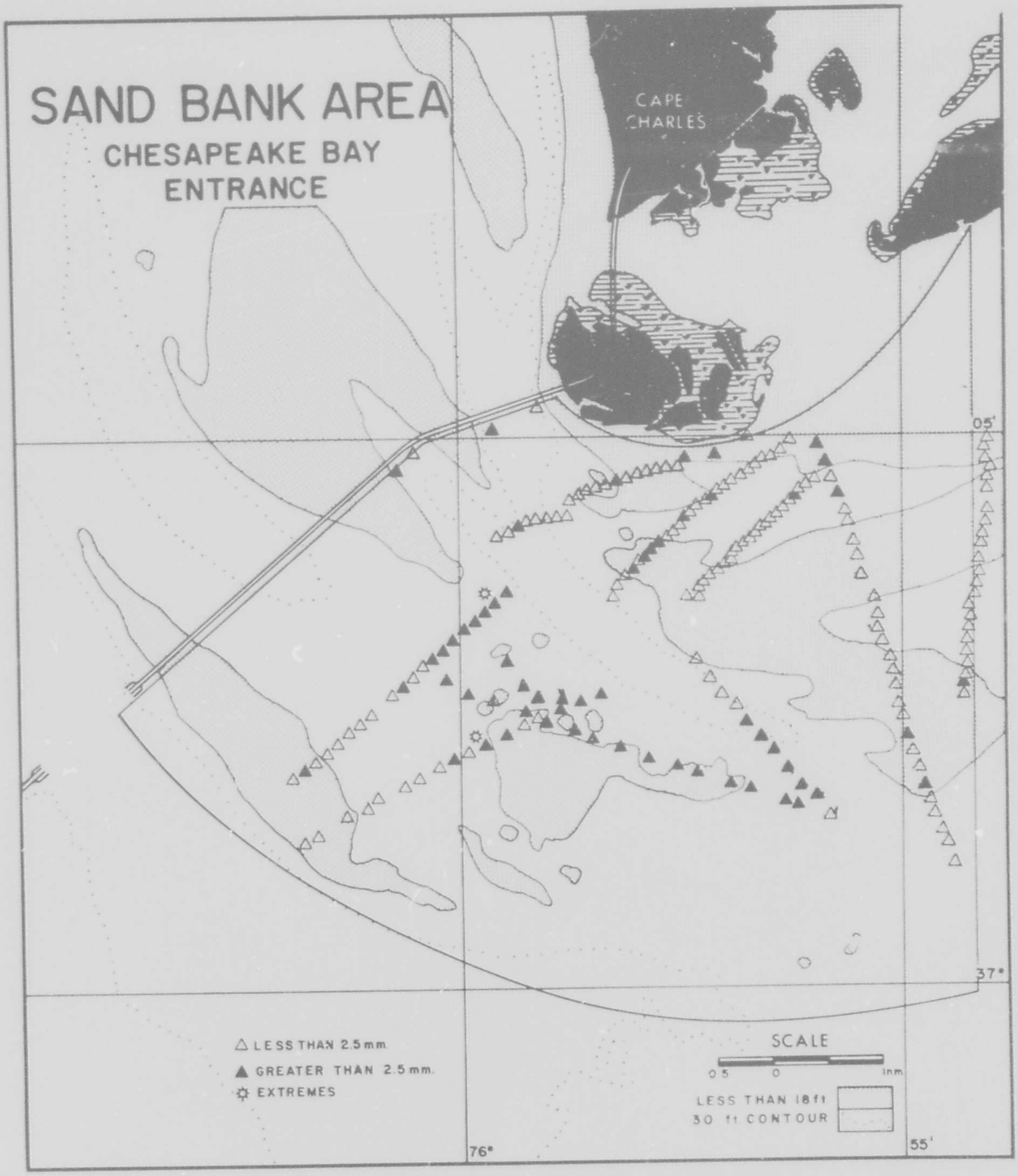
SAND BANK AREA
CHESAPEAKE BAY
ENTRANCE
CAPE
CHARLES
05'
37°
76°
55'
△ LESS THAN 2.5 mm.
▲ GREATER THAN 2.5 mm.
☼ EXTREMES
SCALE
0.5 0 1nm
LESS THAN 18ft
30 ft CONTOUR

TABLE I

Sample Number	(1) Coarsest Grain (mm)	(2) Coarsest Shell (mm)	(3) Wt. % "Fines"	(4) Water Depth (ft.)	(5) Z Score
1-1	2.04	4.59	2.69	39.0*	1.6477
1-3	3.38	13.90	2.79	36.0*	4.6308
1-5	0.89	3.06	3.86	28.0*	-0.2643
1-6	3.66	3.01	1.61	24.0*	4.1307
2-9	4.72	4.72	1.38	27.0	5.5878
2-10	4.68	9.05	1.69	25.0*	5.4190
2-11	5.10	6.97	0.98	23.9	6.2288
2-12	2.51	7.23	1.00	23.0	2.8722
2-13	3.49	8.54	0.80	24.0	4.2085
2-14	2.93	11.22	1.54	24.0*	3.2230
2-15	6.76	11.39	1.06	23.0	8.3407
2-16	4.34	8.63	1.32	19.0*	5.1156
2-17	3.91	8.93	1.03	24.0*	4.6731
2-18	4.63	10.67	1.11	24.8	5.5771
2-19	3.74	11.48	0.96	24.0	4.4791
2-20	5.73	9.65	1.15	23.0*	6.9899
2-21	7.48	16.66	1.71	23.8	9.0354
2-22	3.06	7.57	1.34	23.0*	3.4611
2-23	2.38	2.93	1.01	22.8	2.7038
3-24	1.66	9.27	1.61	28.0*	1.5501
3-25	0.89	8.84	1.97	30.6	0.4296
3-26	1.83	11.98	2.21	34.0	1.5494
3-27	3.10	7.99	2.66	35.6	3.0313
3-28	2.08	11.69	2.03	36.1	1.9266
3-29	0.89	5.61	1.66	34.1	0.5434
3-30	1.62	5.02	1.63	30.7	1.4878
3-31	2.00	4.93	1.96	27.1	1.8608
3-32	1.28	1.87	0.97	23.6	1.2909
3-33	0.77	5.18	1.69	21.6	0.5880
3-34	0.68	2.21	0.93	21.9	0.5369
3-35	0.72	3.57	1.66	20.1	0.3238
3-36	0.72	3.15	0.87	19.1	0.6139
3-37	1.15	2.51	0.87	17.6	1.1629

(1) Intermediate diameter of coarsest grain (mm).

(2) Intermediate diameter of coarsest shell (mm).

(3) Weight percentage of material finer than 0.062 mm.

(4) Water depth (ft.)

(5) Z Score based on discriminant function developed from coarsest grain and weight percentage "fines" measurements.

*Accurate to ± 2 feet.

TABLE I (continued)

Sample Number	(1) Coarsest Grain (mm)	(2) Coarsest Shell (mm)	(3) Wt. % "Fines"	(4) Water Depth (ft.)	(5) Z Score
3-38	1.06	3.91	0.98	16.7	1.0127
3-39	1.02	3.57	1.00	16.6	0.9505
3-40	1.02	1.83	0.99	16.6	0.9542
3-41	0.98	2.76	1.14	17.2	0.8442
3-42	0.94	6.93	1.04	17.2	0.8260
3-43	1.19	4.46	0.98	18.2	1.1775
3-44	1.02	1.49	0.98	18.2	0.9578
3-45	0.98	5.44	1.34	18.7	0.7966
3-46	0.81	2.30	1.01	19.7	0.6723
4-47	1.49	3.87	1.69	31.0	1.3011
4-48	2.13	7.82	1.49	29.5	2.1981
4-49	2.17	7.86	1.13	30.0	2.3852
4-50	3.49	8.29	1.02	28.0	4.1277
4-51	2.04	6.55	0.82	29.0	2.3343
4-52	3.91	8.29	0.84	29.0	4.7428
4-53	5.06	10.71	0.83	28.0	6.2290
4-54	4.34	9.69	0.80	28.0	5.3066
4-55	0.98	4.17	1.62	25.0	0.6679
4-56	2.30	6.84	0.83	25.0	2.6601
4-57	2.04	6.38	1.04	29.5	2.2535
4-58	2.72	3.87	1.00	25.0	3.1467
4-59	1.74	5.10	1.35	28.5	1.5718
4-60	1.83	3.91	1.68	30.6	1.7440
4-61	1.32	4.85	1.55	31.6	1.1329
4-62	2.85	3.61	1.76	32.6	3.0324
4-63	0.98	2.13	1.83	31.1	0.5908
4-64	1.70	6.72	2.02	29.1	1.4544
4-65	1.28	4.63	2.32	28.6	0.7952
4-66	1.36	6.21	2.31	26.1	0.9087
4-67	0.77	3.49	2.74	23.6	-0.0178
4-68	0.81	3.61	7.59	20.6	-1.7438
4-69	2.30	8.84	2.12	17.1	2.1864
4-70	1.57	10.12	1.85	14.1	1.3521
4-71	2.13	10.63	2.05	11.6	1.9925
5-72	1.28	5.74	1.11	19.1	1.2395
5-73	2.64	5.06	1.12	19.1	2.9928
5-74	0.64	2.13	0.78	20.1	0.5371
5-75	1.40	4.21	0.93	20.3	1.4703
5-76	1.11	2.89	0.94	14.3	1.0823
5-77	0.89	4.21	0.69	21.3	0.8996
5-78	0.94	4.08	1.27	23.3	0.7415
5-79	2.08	4.29	0.79	27.3	2.4002
5-81	4.21	11.56	1.20	29.3	4.9950
5-82	1.49	9.01	1.85	29.3	1.2423

TABLE I (continued)

Sample Number	(1) Coarsest Grain (mm)	(2) Coarsest Shell (mm)	(3) Wt. % "Fines"	(4) Water Depth (ft.)	(5) Z Score
5-83	1.62	5.10	2.22	28.3	1.2712
5-84	2.51	9.10	2.09	28.3	2.4719
5-85	5.19	14.83	2.79	25.3	5.6740
5-86	5.23	14.24	3.00	25.3	5.6518
5-87	4.29	7.44	2.09	27.4	4.7780
5-38	3.36	4.29	1.46	25.4	3.8014
5-89	3.49	5.61	1.93	25.4	3.7935
5-90	5.61	6.12	0.97	22.4	6.8913
5-91	8.59	16.36	1.59	22.4	10.5071
5-92	5.87	9.94	1.05	25.4	7.1914
6-93	1.06	6.33	1.08	20.3	0.9760
6-94	1.40	6.04	0.95	17.3	1.4630
6-96	1.36	5.99	1.37	29.3	1.2539
6-97	1.57	5.99	0.84	17.3	1.7230
6-98	1.32	5.02	1.00	15.3	1.3348
6-99	0.98	4.25	1.29	17.3	0.7891
6-100	1.66	5.48	0.89	17.3	1.8145
6-101	1.36	5.57	0.90	18.3	1.4265
6-102	2.59	5.02	1.03	17.3	2.9710
6-103	1.11	6.76	1.76	16.3	0.7812
6-104	8.12	9.27	0.34	16.3	10.3621
6-105	5.61	7.06	0.15	16.3	7.1924
6-106	2.08	5.31	1.85	15.3	2.0110
6-107	1.57	7.44	0.81	15.3	1.7340
6-108	3.02	4.72	1.68	15.3	3.2814
6-109	3.49	8.54	1.22	13.3	4.0542
6-110	6.72	7.86	1.16	12.3	8.2491
7-111	0.85	2.72	7.55	37.8	-1.6742
7-112	0.93	3.06	2.70	28.8	0.2100
7-113	2.68	8.50	2.20	28.8	2.6512
7-114	1.15	6.33	8.32	33.8	-1.5726
7-115	1.36	4.97	1.97	36.3	1.0335
7-116	1.79	4.76	1.94	38.0	1.5936
7-117	2.21	8.24	1.09	43.0	2.4548
7-118	1.53	6.84	1.17	47.0	1.5469
7-119	0.85	2.89	1.38	19.0	0.5913
7-120	1.61	4.63	1.01	15.0	1.7155
7-121	0.81	3.78	0.86	15.0	0.7274
7-122	2.00	6.55	0.73	15.0	2.3125
7-123	0.94	8.46	1.11	17.0	0.8003
7-124	2.93	8.50	0.93	21.0	7.3227
7-125	1.36	4.29	1.07	20.0	1.3650
7-126	1.36	4.76	1.80	23.0	1.0960
7-127	0.81	3.91	3.21	21.0	-0.1355

TABLE I (continued)

Sample Number	(1) Coarsest Grain (mm)	(2) Coarsest Shell (mm)	(3) Wt. % "Fines"	(4) Water Depth (ft.)	(5) Z Score
7-128	1.01	3.99	3.35	19.0	0.0876
7-129	0.94	4.85	3.53	16.0	-0.0882
7-130	2.00	3.91	2.21	17.0	1.7690
7-131	3.44	7.99	1.78	19.0	3.7937
8-132	1.79	6.72	1.84	20.0	1.6303
8-133	2.38	7.74	1.56	20.0	2.5018
8-134	3.65	18.95	1.79	21.0	4.0646
8-135	2.12	8.50	2.37	22.0	1.8750
8-136	2.25	7.27	2.18	23.0	2.1095
8-137	1.66	5.91	2.28	24.0	1.3041
8-138	1.70	6.04	2.18	24.0	1.3957
8-139	0.89	5.31	2.45	25.0	0.2533
8-140	0.60	4.89	5.26	26.0	-1.1627
8-141	0.72	3.14	3.66	22.0	-0.4105
8-142	0.81	3.83	2.22	20.0	0.9624
8-143	0.94	3.87	1.98	16.5	0.4808
8-144	0.55	3.49	1.70	15.0	0.0895
8-145	0.60	3.44	1.23	13.5	0.3170
8-146	0.85	5.70	1.64	13.0	0.4959
8-147	1.19	8.29	2.18	13.5	0.7368
8-148	0.89	3.49	1.24	12.0	0.6976
8-149	0.81	6.50	1.25	13.9	0.5842
8-150	0.81	4.72	1.31	14.9	0.5621
8-151	0.98	3.99	1.11	15.9	0.8526
8-152	1.36	5.19	1.04	18.9	1.3750
8-153	0.64	7.14	1.76	20.9	0.1773
8-154	1.79	7.01	2.09	15.9	1.5385
8-155	0.77	7.74	2.24	14.4	0.1657
8-156	1.02	5.56	1.81	14.9	0.6531
9-157	1.70	3.78	1.31	25.4	1.7151
9-158	3.19	7.61	0.85	21.7	3.8058
9-159	5.23	11.35	1.06	20.7	6.3641
9-160	6.55	12.03	1.03	29.4	8.0772
9-161	5.44	7.74	1.17	37.9	6.5983
9-162	6.33	16.36	1.48	37.0	7.6374
9-163	4.89	6.89	0.76	15.2	6.0350
9-164	1.83	4.34	0.71	10.4	2.1002
9-165	1.23	4.08	1.10	13.0	1.1883
9-166	2.25	4.63	1.06	13.4	2.5207
9-167	0.85	2.08	0.85	14.7	0.7859
10-168	2.76	8.29	2.53	22.0	2.6398
10-169	1.74	6.08	1.83	25.8	1.5791
10-170	2.51	6.29	19.65	31.4	-3.9760
10-171	2.47	4.34	1.91	31.1	2.4831
10-172	1.79	6.97	1.61	22.0	1.7148

TABLE I (concluded)

Sample Number	(1) Co rsest Grain (mm)	(2) Co rsest Shell (mm)	(3) Wt. % "Fines"	(4) Water Depth (ft.)	(5) Z Score
10-173	1.32	5.82	1.31	15.6	1.2210
10-174	2.13	9.48	1.07	12.4	2.3523
10-175	0.85	2.04	0.99	11.2	0.7345
10-176	1.79	5.14	1.20	10.2	1.8654
10-177	1.74	5.06	1.44	14.9	1.7223
10-178	0.89	3.87	2.33	19.2	0.2974
10-179	0.60	2.47	2.05	21.5	0.0159
10-180	1.15	3.15	2.16	22.3	0.6893
10-181	1.74	4.93	1.58	21.2	1.6709
10-182	2.25	5.10	1.33	19.5	2.4142
10-183	2.04	4.93	1.28	18.9	2.1654
10-184	1.45	3.99	1.15	18.1	1.4445
10-185	3.02	4.76	0.82	18.2	3.5972
10-186	1.91	5.19	0.88	18.8	2.1476
10-187	1.62	8.16	0.89	16.2	1.7596
10-188	3.02	3.74	0.81	15.6	3.6008
10-189	1.91	3.49	1.22	19.2	2.0227
10-190	0.81	2.81	1.67	22.2	0.7972
10-191	0.68	2.04	2.20	27.4	0.0706
10-192	1.14	4.17	2.18	29.8	0.6819
10-193	1.70	4.25	2.29	28.5	1.3553
11-194	3.19	6.08	1.47	19.0*	3.5781
11-195	4.16	6.04	1.23	18.0*	4.9291
11-196	3.87	7.73	1.18	20.0*	4.5631
11-197	3.48	5.99	1.34	20.0*	4.0102
12-198	2.93	6.33	1.89	8.0*	3.0944
12-199	1.36	7.01	2.56	4.0*	0.8169
12-200	2.08	8.84	1.96	5.0*	1.9706
12-201	2.93	9.69	2.24	5.0*	2.9659

TABLE II

Function I

Variables - (1) Coarsest grain, (2) Wt. % "fines"

$\bar{z}$ Brown	= 4.9205
$\bar{z}_0$	= 2.6227
$\bar{z}$ Gray	= 0.9561
Mahalanobis D^2	= 3.9688
F	= 45.46 with 2 and 92 degrees of freedom. Significant at $F_{.05}$.

Function II

Variables - (1) Coarsest grain, (2) Coarsest shell, (3) Wt. % "fines", (4) Water depth

$\bar{z}$ Brown	= 4.0330
$\bar{z}_0$	= 1.5726
$\bar{z}$ Gray	= -0.2167
Mahalanobis D^2	= 4.2498
F	= 23.81 with 4 and 90 degrees of freedom. Significant at $F_{.01}$.

Function III

Variables - (1) Wt. % "fines", (2) Water depth

$\bar{z}$ Brown	= -0.7366
$\bar{z}_0$	= -1.0882
$\bar{z}$ Gray	= -1.3439
Mahalanobis D^2	= 0.6073
F	= 6.96 with 2 and 92 degrees of freedom. This function cannot be considered to be significant.

Functions I and II are examples which exhibit a high degree of discrimination and significance. Function I was chosen to establish discriminatory classes for reasons that are discussed in the text.

Function III is an example which shows low discrimination and very little significance.